

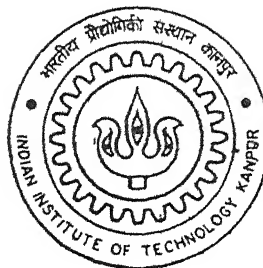
4010107

DEVELOPMENT OF LASER BASED ULTRASONICS DESTRUCTIVE TESTING

By

Sqn Ldr P S SARIN

TH
AE/2002/M
Sa73d



DEPARTMENT OF AEROSPACE ENGINEERING
Indian Institute of Technology Kanpur
JANUARY, 2002

पुष्पसिंह धर्माचार्य / AE
137902

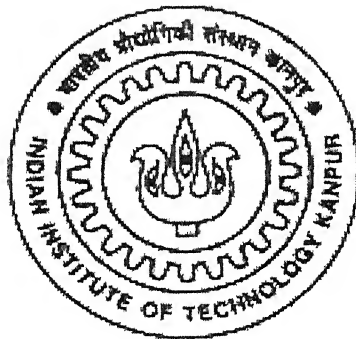


A137902

DEVELOPMENT OF LASER BASED ULTRASONICS NON DESTRUCTIVE TESTING

A Thesis Submitted
in Partial Fulfillment of the Requirements
for the Degree of
MASTER OF TECHNOLOGY

by
Sqn Ldr P S SARIN



to the
DEPARTMENT OF AEROSPACE ENGINEERING
INDIAN INSTITUTE OF TECHNOLOGY KANPUR
JANUARY, 2002



CERTIFICATE

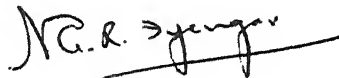
It is certified that the work contained in the thesis entitled “**DEVELOPMENT OF LASER BASED ULTRASONICS NON DESTRUCTIVE TESTING**” by
Sqn Ldr P S SARIN has been carried out under my supervision and that this work has
not been submitted elsewhere for a degree.



Dr. N. N. Kishore

(Professor)

Department of Mechanical Engineering
Indian Institute of Technology, Kanpur.



Dr. N.G.R. Iyengar

(Professor)

Department of Aerospace Engineering
Indian Institute of Technology, Kanpur.

**DEDICATED
TO
MY BELOVED PARENTS**

ACKNOWLEDGEMENTS

I wish to express my gratitude towards my thesis supervisors Dr. N.G.R. Iyengar and Dr. N.N. Kishore for their guidance, invaluable suggestions and constant encouragement.

I wish to express my special thanks to Dr. V. Raghuram, Dr. Atul Kumar Agrawal and Mr. S. K. Rathore for their invaluable suggestions and constant encouragement towards completion of my work.

I appreciate and extend my thanks to my lab mates DaliRaju and Pradipta who worked with me as a team, to ensure the timely commissioning and calibration of the setup. To them and my other labmates, Nitesh, Shashi bhushan and Samuel, I extend my sincere thanks for helping me overcome my inadequacies with respect to computing and computational packages.

I am very much thankful to Shri Trivedi who prepared all test specimens and experimental fixtures in a very short time and professionally. I would be failing in my duty if I do not thank Dr Prashant Kumar and Dr P. Munshi who spared their valuable time to ensure procurement of bought out Scanning equipment and Fixtures.

I would like to thank all my friends for making my stay at IITK very enjoyable and memorable. I will cherish the moments forever.

ABSTRACT

Non Destructive Evaluation (NDE), in particular ultrasonic technique, is an obvious choice for inspection of composites in order to detect macroscopic defects in structures due to its low cost and high reliability. Although piezoelectric transducers are commonly used for nondestructive testing, several problems are associated with the requirement that they be bonded to the test material with an acoustical impedance matching coupling medium. Laser beam ultrasound generation and detection overcomes all of these problems and affords the opportunity to make truly non-contact ultrasonic measurements in both electrically conducting and non-conducting materials, in materials at elevated temperatures, in corrosive and other hostile environments, in geometrically difficult to reach locations, and do all of this at relatively large distances, i.e. meters, from the test object surface.

The present work involves ultrasonic nondestructive evaluation of composite specimens implanted with artificial inclusions like Teflon insert and resin rich zone. A methodology has been proposed using Laser Based Ultrasonics for automated inspection of specimens and evaluation of effectiveness of different features of ultrasonic signal in detecting different types of flaws. Manual C scan image generation using a LBU setup has been implemented. The results achieved are compared with those achieved using a conventional Water submerged ultrasonic setup having fully automated c- scan facility.

The experimentation includes calibration of the laser setup, and includes interfacing of the manual c-scan set-up for scanning composite specimens. In order to investigate various defect modes, both time and frequency domain features have been analyzed. Frequency domain features viz., amplitude at different frequency components, were obtained after performing FFT on the digitized time domain signal. To assess the sensitivity of any single feature or a feature set, C-scan images of the scanned domain were generated by a cluster analysis (Hierarchical clustering with agglomerative procedure). The multidimensional cluster analysis groups the dataset, corresponding to

the selected feature(s) systematically and efficiently. The c-scan image is then generated by assigning each location of the scanned domain with appropriate gray level, depending on the group to which it belongs. A visual comparison of the image with the scanned domain gives a qualitative assessment of the sensitivity of the feature(s) to the defect.

An alternate method of feature extraction using wavelets has also been studied. Discrete Wavelet Transform (DWT) was used for noise suppression from all the acquired signals, by using 'coif5' mother wavelet. By combining the time domain and the classical Fourier analysis, the wavelet transform provides simultaneous spectral representation and temporal order of the signal decomposition components. Construction of a C-scan image from A-scan signals has been implemented by a selection process of wavelet coefficients, followed by an interpretation procedure in the time-frequency domain.

CONTENTS

CERTIFICATE		ii
ACKNOWLEDGEMENTS		iv
ABSTRACT		v
LIST OF FIGURES		x
LIST OF SYMBOLS		xi
CHAPTER 1	INTRODUCTION	1
1.1	Introduction	1
1.2	Literature Survey	3
1.3	Present Work	5
CHAPTER 2	BASICS OF LASER ULTRASONIC TECHNIQUE	7
2.1	Introduction	7
2.2	Basic Principle Of Laser Operation	7
2.3	Main Characteristics Of Laser Light	8
2.3.1	Monochromaticity	8
2.3.2	Coherence	9
2.3.3	Directionality	9
2.3.4	Intensity	10
2.4	Lasers for Ultrasonic Generation	10
2.5	Lasers for Interferometry	11
2.6	Laser-Generated Ultrasound Modes	12
2.7	Methods of Interferometry	13
2.8	He-Ne laser Heterodyne Interferometer	14
2.8.1	Principle of Detection	14
2.8.2	Working of Heterodyne Interferometer (optics)	15
2.8.3	Sensitivity	15
2.9	Closure	16
CHAPTER 3	EXPERIMENTAL SET-UP AND PROCEDURE	18
3.1	Experimental Setup(LBU)	18
3.1.1	Nd: YAG Pulsed Laser Ultrasonic Generator	18
3.1.2	Optical Heterodyne Laser (He-Ne) Probe	19
3.1.3	Digital Storage Oscilloscope	19
3.1.4	Computer	19
3.2	Experimental Procedure (LBU)	20
3.2.1	Installation And Calibration Of Setup	20

	3.2.2	Preparation Of Specimen	21
	3.2.3	Scanning Procedure	21
3.3		Experimental Setup (Conventional)	22
	3.3.1	Scanning tank	22
	3.3.2	Ultrasonic flaw detector	22
	3.3.3	Computer	23
	3.3.4	Stepper motor and Controller	23
	3.3.5	Analog to Digital Converter	23
	3.3.6	Transducers	24
3.4		Experimental Procedure	24
3.5		Closure	25

CHAPTER 4 **BASICS OF SIGNAL PROCESSING, WAVELETS 29** AND CLUSTER ANALYSIS

4.1		Introduction	29
4.2		Digital Signal Processing	30
	4.2.1	Digitizing the Time Axis	30
	4.2.2	Digitizing Signal Amplitude	31
	4.2.3	Time and frequency	31
	4.2.4	Short Time Fourier Analysis (STFA)	32
4.3		Wavelet Analysis (WA)	32
	4.3.1	Continuous Wavelet Transform (CWT)	33
	4.3.2	Discrete Wavelet Transform (DWT)	34
	4.3.3	Multi Resolution Analysis (MRA)	34
	4.3.4	Multiple-Level Decomposition	35
	4.3.5	Wavelet Reconstruction	35
	4.3.6	Properties of Wavelets	35
	4.3.7	Different types of Wavelets	36
4.4		Noise Suppression	36
4.5		Data Compression	37
	4.5.1	C- scan image generation	39
4.6		Basics Of Cluster Analysis	39
	4.6.1	Hierarchical Tree	40
	4.6.2	Distance Measures	40
		4.6.2.1 Euclidean distance	41
		4.6.2.2 Squared Euclidean distance.	41
		4.6.2.3 City-block (Manhattan) distance	41
		4.6.2.4 Chebychev distance	42
		4.6.2.5 Power distance	42
		4.6.2.6 Percent disagreement	42
	4.6.3	Amalgamation or Linkage Rules	42
		4.6.3.1 Single linkage (nearest neighbor).	43
		4.6.3.2 Complete linkage (furthest neighbor)	43
		4.6.3.3 Unweighted pair-group average	43

	4.6.3.4	Weighted pair-group average	43
	4.6.3.5	Unweighted pair-group centroid.	44
	4.6.3.6	Weighted pair-group centroid.	44
	4.6.3.7	Ward's method	44
	4.6.4	Using Distances to Group Objects	45
	4.6.5	Hierarchical clustering	45
	4.6.6	Non Hierarchical clustering	45
4.7		Present Study	46
4.8		Closure	49
CHAPTER 5		RESULTS AND DISCUSSION	56
5.1		Experiment Details	56
5.2		Cluster Analysis	56
5.3		Wavelet Analysis	58
5.4		Closure	59
CHAPTER 6		CONCLUSIONS AND SCOPE FOR FUTURE WORK	77
6.1		Conclusions	77
6.2		Scope For Future Work	77
REFERENCES			79
Appendix A			81
Appendix B			82
Appendix C			83
Appendix D			84
Appendix E			86

List of Figures

2.1 Optical Layout of Heterodyne Interferometer.	17
3.1 Schematic layout of Experimental setup (LBU)	26
3.2 Photograph of Experimental setup (LBU)	27
3.3 Schematic layout of Experimental setup (Conventional Ultrasonics)	28
4.1 Fourier Transform for transforming a time-domain signal to frequency-domain.	50
4.2 Short time Fourier Transform and Wavelet Transform	50
4.3 Scaling of the wavelets with different scale factors	50
4.4 Shifting of the wavelets with different shift parameters	51
4.5 Multiple Level Wavelet decomposition tree with three level decomposition	51
4.6 Different wavelets, scaling and wavelet functions	52
4.7 Hierarchical Tree Plot	55
5.1 Diagrammatic representation of Specimens.	60
5.2 Signals recorded by LBU	61
5.3 C-scan Images generated by Cluster Analysis	66
5.4 Signals recorded using pre-amplification facility in LBU	70
5.5 Signals recorded with fluctuation in incident laser energy	73
5.6 C-scan images generated by Wavelet Analysis	74
5.7 Additional defects in specimens picked up by wavelet and clustering techniques.	76

List Of Symbols

E_k	The within group error sum of squares
x_{ijk}	The data belonging to i^{th} of n variables for the j^{th} of m_k data units in the k^{th} of h clusters.
\bar{x}_{ik}	The mean on the i^{th} variable for m_k data units in the k^{th} cluster
Ω_s	The sampling frequency
$f(t)$	Signal
t	Time
τ	Time-shift
ω, ν	Frequency
$F(\omega)$	Signal in frequency-domain
$w(t-\tau)$	Window function
a	Scaling parameter
b	Translation parameter
$F(\omega)$	Fourier Transform
$W_f(a, b)$	Wavelet Transform
$\psi(t)$	Mother wavelet function
$C(a, b)$	Wavelet coefficient
$s(t)$	Ultrasonic signal
$y(t)$	De-noised signal
$n(t)$	Noise
$S(t)$	De-noised multi path (overlapped) signal
$R(t)$	De-noised reference signal
$f(n)$	Digitized sequence of signal $f(t)$ at the scale 2^j
d_j	The approximation of $f(n)$
Wf	Vectorial wavelet representation of $f(n)$
\hat{m}_j	Wavelet coefficient mean
$C_{x,y}$	Characterization parameter of the signal $r_{x,y}(t)$

INTRODUCTION

1.1 INTRODUCTION

Non-Destructive testing and Evaluation (NDE) techniques play a major role in quality assurance of structural members during manufacturing stage and operating life. Ultrasonic testing is one of the most promising techniques both due to its effectiveness and simplicity of setup. Ultrasonic Inspection involves impinging a low energy, high frequency stress pulse into the material under inspection and examining the subsequent propagation of this energy. Defects such as cracks and inclusions act as sources of wave scattering through reflection, refraction, diffraction and mode conversion. Being one of the most commonly used Non Destructive Testing (NDT) methods, Ultrasonic Testing (UT) is developing rapidly in recent years. The UT method uses ultrasonic waves for detection and sizing of internal defects of materials. In this, a piezo-electric transducer (probe) generates ultrasonic waves, which propagate in the elastic medium and are detected either by the same (Pulse echo) or by a different transducer (Through transmission).

Although piezoelectric transducers are commonly used for nondestructive testing, several problems are associated with the requirement that they be bonded to the test material with an acoustical impedance matching coupling medium. For velocity measurements, which are necessary for material thickness measurements and to locate the depth of defects, the coupling medium can cause transit time errors. Due to partial transmission and partial reflection of the ultrasonic energy in the couplant layer, there may be a change of shape of the waveform, which can further affect accuracy of the velocity measurement. This can also lead to serious errors in absolute attenuation measurements, which is the reason that so few reliable absolute measurements of attenuation are reported in the scientific literature. Therefore, a method of non-contact generation and detection of ultrasound is of great practical importance. Several such techniques are presently available in various stages of development, namely capacitive

pick-ups, electromagnetic acoustic transducers (EMATs), laser beam optical generators and detectors, and more recently air (gas)-coupled ultrasonic systems. However, as the name implies, capacitive pick-ups cannot be used as ultrasonic generators and, even when used as detectors, the air gap required between the pick-up and test structure surface is extremely small, which in essence causes the device to be very nearly a contact one. One major problem with EMATs is that the efficiency of ultrasound generation and detection rapidly decreases with lift-off distance between the EMATs face and the surface of the test object. They can obviously be used only for examination of electrically conducting materials. Because of the physical processes involved they are much better detectors than generators of ultrasound. Laser based ultrasound (LBU) generation and detection overcomes all of these problems and affords the opportunity to make truly non-contact ultrasonic measurements in both electrically conducting and non-conducting materials, in materials at elevated temperatures, in corrosive and other hostile environments, in geometrically difficult to reach locations, and do all of this at relatively large distances, i.e. meters, from the test object surface. Furthermore, lasers are able to produce simultaneously shear and longitudinal bulk wave modes as well as Rayleigh and plate modes. These systems have been used to inspect aircraft structures, art paintings, lumber, composite pre-pregs, and composite panels. LBU uses a pulsed laser to generate the ultrasound and a continuous wave (CW) laser interferometer to detect the ultrasound at the point of interrogation to perform ultrasonic inspection.

The various pops and bursts that appear in a sensor output have physical causes, and in ultrasonic observations, the physics of the causes is typically well understood. Signal processing must exploit this understanding to bring the maximum of new and relevant meaning from the sensor output data, and to provide an indication of confidence in the results. Once the signature of interest is separated from everything else in the sensor signal, the detection of flaws in a work piece is straightforward. Typically, the work piece is scanned across a physical range by the sensor. Continuity of the mathematical properties of the signature across scans suggests an unflawed work piece. The appearance of an abrupt discontinuity suggests the presence of a flaw.

The possibility of employing wavelet analysis in ultrasonic nondestructive applications has been studied since the beginning of the eighties, giving interesting results at least in laboratory applications. The Wavelet Transform (WT) divides the signal into different frequencies/scales/levels in terms of basis functions obtained by compression/dilatation and translation of mother wavelet. Compared to other time-frequency representations like short time Fourier transform and Wigner-ville transform, the wavelet transform provides spectral representation and temporal order of the signal components simultaneously. Another important property is that the signal reconstruction does not involve global averaging in time or frequency domains because of good localization of the wavelet coefficients in both domains.

1.2 LITERATURE SURVEY.

In ultrasonic techniques, information on defect characterization requires more evolved techniques than classical methods. Modern non-destructive testing of materials has to provide the highest possible detection probability, the correct size and exact orientation of defects in the specimen. The simplest acoustical characterizations of materials deal with velocity measurements. Some well-known techniques of calculating wave speed by measuring the time-of-flight are described in Krautkramer and Krautkramer [1]. Neslroth et al [2] introduced the idea of using various features of ultrasonic signal to detect various types of defects, flaws or anomalies in composite materials. Rose [3] introduced a concept of feature mapping. The basic concept is based on the fact that different types of defects are expected to interact distinctively with different features of ultrasonic signal. Rose [3] proposed the Fischer linear discriminant function as the classifier, which uses a linear combination of useful features to detect anomalies. Debasis [4] proposed a methodology to experimentally detect defects using a two-dimensional automated Ultrasonic C-scan system. Both time and frequency domain features were extracted from the digitized data during scanning procedure. Multidimensional cluster analysis was used for effective grouping of datasets in a systematic manner leading to automatic image generation. Detection of ultrasound by optical means were motivated by the need to visualise and image the ultrasonic field. Scruby and Drain [5] in their introductory book

on this subject have elaborated on the principles underlying generation and reception processes of all techniques used. Monchalín [6] has given an elaborate review on discussion of different techniques with reference to exploitation of the power of the laser ultrasonic generation. The review covers knife-edge techniques, optical heterodyning, differential interferometry, and velocity (time-delay) interferometry methods. Huber and Green [7] in their publication have elaborated on the design of a portable fiber-optic heterodyne interferometer for detection of out-of-plane motion on the surfaces. They had successfully coupled this detection system with a compact Nd: YAG laser for generation of ultrasonic waves. Corbel et al [8] showed that a pulsed laser can be used to generate simultaneously elastic waves of different types in laminate composite materials. Huang et al [9] showed that a laser based ultrasonic system consisting of a tunable narrowband laser line array ultrasound generator and a fiber-optic dual probe heterodyne interferometer can be used for detection of cracks and for tomographic imaging in thin plates. Castegnede et al [10] reviewed some advances dealing with the characterisation of composite materials by using laser based ultrasound techniques. They discussed laser interferometer detection and the determination of the theoretical displacement fields. Cho et al [11] carried out an evaluation of subsurface lateral defects, using SAW (surface acoustic waves) generated by a Q-switched YAG laser and monitored by a heterodyne laser interferometer. This fundamental work was carried out on thin metallic foil, the material's properties of bonded layer can be estimated by the velocity dispersion of the Rayleigh wave, and the bond Quality can be estimated by an analysis of the generalised lamb wave. Yamawaki et al [12] also demonstrated the applicability of using LBU technique for a microscopic material evaluation in imaging experiments using specimens, which contain artificial subsurface defects. Independent component analysis and feature extraction techniques for NDT data have been compared by Carlo [13] in his paper, which also proposes a combination of various types of features to cope with different situations. Rathore et al [14] have employed LBU and ray acoustics for establishing a criterion to identify the ray tangential to the defect boundary and evolve a method of reconstruction of the defect to estimate the size and location of the defect. Legendre et al [15] have proposed a wavelet-based method to perform the analysis of NDE ultrasonic

signals received during the inspection of reinforced composite materials. By combining the time domain and the classical Fourier analysis, the wavelet transform provides simultaneous spectral representation and temporal order of the signal decomposition components. To construct a C-scan image from A-scan signals they proposed a selection process of wavelet coefficients, followed by an interpretation procedure in the time-frequency domain.

This study is carried out based on a-priori knowledge of the defect and uses windowing technique on data generated by pulse echo mode. A technique needs to be established for finding defects which does not call for a-priori knowledge, and does not take recourse to multiple iterations, to check for defects at different depths within the specimen as is done by the technique proposed by Legendre et al [15]. Such a methodology would be ideally suited for use in a portable NDE equipment based on laser Ultrasonics. Detailed investigations on exact extent/location of defects could follow, once existence of defects with high order of reliability is ensured.

1.3 PRESENT WORK

The present investigation involves ultrasonic nondestructive evaluation of composite specimens implanted with artificial inclusions like Teflon inserts and also resin rich zones. In the present work, an experimental setup has been developed using an Nd: YAG pulsed laser for generation of ultrasonic waves in specimens and a He-Ne continuous laser based heterodyne optical interferometric probe for detection of the same. A methodology has been proposed for using Laser Based Ultrasonics for inspection of composite specimens and evaluation of effectiveness of different features of ultrasonic signal in detecting different types of flaws. Manual C scan image generation using a LBU setup has been implemented.

The experimentation includes calibration of the laser setup, and interfacing of the manual c-scan set-up for scanning composite specimens. The basic purpose of the c-scan setup, developed in house, is to scan a predefined region of the component, digitize and extract different features from the ultrasonic waveform at each point scanned.

Specimens were prepared with known flaws such as Teflon insert and resin rich zones created during fabrication. For investigation of various defects, both time and frequency domain features have been analysed. Frequency domain features viz., amplitude at different frequencies was obtained after performing FFT on the digitized time domain signal. To assess the sensitivity of any single feature or a feature set, C-scan images of the scanned domain were generated by a cluster analysis (Hierarchical clustering with agglomerative procedure). The multidimensional cluster analysis groups the dataset, corresponding to the selected feature(s) systematically and efficiently. The C-scan image is then generated by assigning each location of the scanned domain with appropriate gray level, depending on the group to which it belongs. A visual comparison of the image with the scanned domain gives a qualitative assessment of the sensitivity of the feature(s) to the defect.

An alternate method of feature extraction using wavelets has also been studied. By combining the time domain and the classical Fourier analysis, the wavelet transform provides simultaneous spectral representation and temporal order of the signal decomposition components. Construction of a C-scan image from A-scan signals has been implemented by a selection process of wavelet coefficients, followed by an interpretation procedure in the time-frequency domain. The results achieved by both methods using the new LBU technique is compared with those achieved using a conventional Water submerged ultrasonic setup having fully automated c- scan facility.

The presentation is given in details in different chapters. Chapter 2 discusses, the various aspects of laser excited ultrasonic technique (LBU). In Chapter 3, the details of the experimental setup and data acquisition procedure are discussed. Chapter 4 presents Cluster analysis, the wavelet analysis and signal analysis techniques. Chapter 5 presents the results and discussion, with reference to earlier findings and in the context of strengths and limitations of the methods/analysis techniques used. Chapter 6 covers the conclusions of the present work and suggestions for the future work.

BASICS OF LASER ULTRASONIC TECHNIQUE

2.1 INTRODUCTION

In the field of nondestructive evaluation, the need to detect defects has motivated extensive work on the interaction of laser generated ultrasonic waves with natural and artificial flaws. Laser generation and detection of defects is potentially useful to investigate a wide range of materials. The main advantage of using laser based rather than conventional piezoelectric transducers is that this technique does not require any direct mechanical contact with the inspected body. At a sufficiently low absorbed power density, the acoustic waves are generated by the thermoelastic expansion and other methods. In the thermoelastic regime, a pulsed laser offers a wideband reproducible source. An optical interferometer is used as a large bandwidth (0.01-20 MHz) non-contact point detector of the surface displacement associated with the ultrasonic wave. The probe can be used to detect displacements as small as 1 Å .

2.2 BASIC PRINCIPLE OF LASER OPERATION.

The laser is a device, which amplifies the intensity of light by means of a quantum process known as stimulated emission. Indeed the name LASER is an acronym standing for Light Amplification by Stimulated Emission of Radiation. In what follows, some details are presented for the sake of continuity. The operation of the simplest laser can be readily understood in terms of a quantum mechanical model having say three energy levels E_0 , E_1 , E_2 , such that $E_2 > E_1 > E_0$. In reality, there may be more than three levels. The ground state is well populated, whereas the intermediate and upper states are sparsely populated. Now an atom absorbs energy in terms of quantum theory and is excited into the upper state, the radiation having a frequency ν_p such that

$$h\nu_p = E_2 - E_0$$

Where h is the Planck's constant. In laser terminology this process is called 'pumping', so that ν_p is the 'pumping frequency'. Pumping tends to equalize the population of two states so that E_2 becomes well populated. Emission can now occur in response to incident radiation, at a frequency ν given by

$$h \nu = E_2 - E_1.$$

Note that necessarily $\nu \geq \nu_p$, so that the pumping frequency must always be equal to or higher than that of the radiation to be amplified. In order to obtain light of sufficient intensity for practical use, there has to be some mechanism for feeding the energy back into the laser system and thereby building up the amplitude of oscillations in a resonant system. The usual way of obtaining sustained oscillations is to site a high performance mirror at each end of the lasing medium. In the simplest system both mirrors are plane, and accurately aligned perpendicular to the axis of the laser. Thus the light is reflected backwards and forwards through the lasing medium. On each pass it stimulates further emission from the medium and is thus amplified in intensity.

2.3 MAIN CHARACTERISTICS OF LASER LIGHT

Laser is characterized by a number of key optical properties, most of which play an important role in the generation of ultrasonic waves. Their four major optical properties are:

- (1) Monochromaticity
- (2) Coherence
- (3) Directionality
- (4) Intensity

2.3.1 Monochromaticity

Monochromaticity of a laser is reduced by multimode operation of a laser. A small He-Ne laser generally has 3-4 longitudinal modes excited with a spacing of a few hundred MHz, depending on the cavity length. This still gives a bandwidth of a few parts in 10^6 . Solid-state lasers tend to have rather large frequency spreads. Monochromaticity is

important for some ultrasonic applications, in particular the interferometric measurement of ultrasonic fields.

2.3.2 Coherence

Coherence is an important property when it comes to building an optical system to detect ultrasonic waves. In simple words coherence is used to describe how well a wave disturbance at one point in space or time correlates with the disturbance at another point. If there is a well defined phase relationship between the light at two different points in space (i.e. two light beams), or at two different times (i.e. one beam split into two with a delay between the parts, as is typical in an interferometer) than the two light disturbances can be brought together to produce a predictable interference pattern. If the light is completely incoherent so that there is no predictable relationship (i.e. random phase) between the two disturbances, no interference fringes will be formed.

Most techniques involve some form of interferometer, in which good coherence between the reflected and reference beam is essential. Coherence length is the distance of the origin of the beam to the farthest point at which the wave disturbance can be effectively correlated with the disturbance at its starting point. Conventional monochromatic light cannot be used because their coherence length is only of the order of millimeters. The use of a gas laser however enables use of a longer probe than reference beam. This means that a compact instrument (incorporating all except the probe beam) can be built, and that the distance to the sample is not critical.

2.3.3 Directionality

Directionality is a function of the spatial coherence of the beam of light. The radiation produced by a laser is confined to a narrow cone of angles. The beam divergence for a typical gas laser is of the order of 1 milliradian. Commercial He-Ne lasers having divergence of a few tenths of a milliradian are also available. The diameter of the beam is typically about 1mm for a gas laser such as helium-neon, and in the range 1-20mm for a pulsed solid-state laser. The light from gas and solid state lasers thus forms a highly collimated beam which is extremely valuable for laser ultrasonics since it enables the beam to be focused to a very small spot. This means not only high spatial resolution, but

also, in the case of ultrasonic displacement measurement by interferometer, the ability to collect a larger fraction of the scattered light from a rough surface, thereby increasing the sensitivity. For laser generation it means that very high incident power densities are attainable. Low beam divergence also means that the beam can travel distances of the order of several meters from the laser to the specimen without appreciable spreading and losses. Thus both laser generation and reception of ultrasound can be made genuinely remote techniques.

2.3.4 Intensity

This is the property for which lasers are best known outside the field of optics. Although the optical power output from a small helium-neon (He-Ne) laser may be only say 2mW, a beam diameter of 0.5mm leads to a power density of about 1 Wcm^{-2} . Such a beam can be readily focused by a simple lens to a spot of diameter 0.05 mm because it is monochromatic and coherent. The incident power intensity is then 100 Wcm^{-2} .

Intensity is a very important property for laser reception of ultrasound, as sensitivity of a single mode laser interferometer system (defined as signal to noise ratio for a fixed bandwidth) increases with the square root of light intensity, provided other conditions remain constant. The limiting factor becomes the intensity at which the specimen is damaged or otherwise adversely affected by intense irradiation. Increase in power also brings penalties like increase in noise and multimode interference. Intensity is also a crucial factor in the generation of ultrasound by laser since incident power intensities typically in the range of 10^4 - 10^6 Wcm^{-2} are needed to act as a thermoelastic source of ultrasound.

2.4 LASERS FOR ULTRASONIC GENERATION

The simple laser arrangement will operate in a pulsed mode if it is pumped for example by a pulsed flash tube. Depending on the type of laser, pulses of duration typically 100 μs to 1ms can be obtained. Although high-energy pulses can be produced in this way, the normal mode is not particularly useful for laser ultrasonics because the pulse duration is too large. An additional technique, known as Q- switching or Q-spoiling, is needed to

obtain pulses in the required 1-100ns range. The Q (quality) factor of a cavity resonator is the energy stored in the cavity divided by the energy lost from the cavity per round trip of the light within the cavity. Thus if Q is low the cavity oscillations are suppressed and the stored energy builds up within the lasing medium. When the Q is high, the cavity can support oscillations into which energy is supplied from the medium. Thus switching from low to high Q results in the rapid extraction of power from the laser cavity. Practical Q-switches are in the form of elements with variable absorption that are inserted between the mirrors. Two commonly used Q switches are the Pockels cell and bleachable (saturable) dye. Also of potential importance to non-contact ultrasonics are lasers that can be pulsed repetitively. Adequate cooling in pulsed solid-state laser is a problem. Hence gas lasers are preferred. However solid-state lasers can store higher individual pulse energies than gas medium lasers. Conventional ultrasonic inspection often uses palpitation rate as high as 1-10 kHz for signal averaging purposes or for speed.

Laser generation of ultra sound does not impose very stringent conditions on the source laser. All that is required is the ability to deliver a reasonably high pulsed energy density to a small area of the specimen, where the pulse length are in the range of 1-100ns. As already mentioned, wavelength is not critical, nor is monochromaticity and coherence. Most researchers have employed a solid state laser, either ruby or Nd:YAG. The Nd:YAG laser has proved itself to be a versatile system under Q-switched conditions. However, the fundamental wavelength (1064nm) is in the near infrared, which makes alignment more difficult than with the visible laser. The frequency-doubled wavelength of 532 nm is in the visible spectrum while the harmonics of 266nm and 355nm are in the ultraviolet zone.

2.5 LASERS FOR INTERFEROMETRY

For applications like interferometry, where wavelength purity and coherence are important, continuous wave lasers are to be designed with special optical components. The main problem is that a simple laser will excite a number of longitudinal and transverse modes. The result is that energy is amplified over a narrow range of frequencies instead of the desired single frequency, giving rise to inter mode beat frequencies, and there is a variable distribution of energy across the beam. The generally

preferred transverse mode (usually the lowest order mode with circular symmetry, TEM_{00}) can be selected, and higher order modes suppressed, by the use of at least one curved (concave) mirror at the end of the cavity and/or a suitable aperture within the cavity. A multimode laser can be employed to minimize the multi-mode problem of longitudinal wavelengths in interferometry and then a balanced detection system and adjustment of the path difference between the two arms of the interferometer can be used to minimize the effects of intermode beats if necessary.

The recording of ultrasonic waves by laser is dependent upon all the fundamental properties of the laser: monochromaticity, coherence, directionality and power density. Because of its ready availability and excellent optical characteristics, notably monochromaticity and coherence, the helium-neon laser is mostly used. This system is however somewhat limited with regard to maximum power which controls sensitivity. The argon ion laser delivers higher power and is also inherently more sensitive because of its shorter wavelength. Argon ion lasers are however very noisy. Nd:YAG laser is also suitable for application in laser interferometers.

2.6 LASER-GENERATED ULTRASOUND MODES

The use of a pulsed laser to generate broadband acoustic signals is now well established; three basic mechanisms of ultrasonic generation have been identified:

- (I) The thermoelastic regime. Absorption of a low power pulse causes a rapid localized rise of temperature, which results in a transient (dilatational) thermoelastic stress. Stress components normal to the surface are relaxed at the surface and the stress is approximately biaxial in the plane of the surface. In isotropic materials, elastic waves generated from this type of thermoelastic expansion mechanism are most energetic in a cone inclined at approximately 60° to the surface.
- (II) The constrained surface source. In this regime, the ultrasonic amplitude of the thermoelastic mechanism is enhanced by applying a transparent coating to the irradiated surface. This mechanically constrains the stress relaxation normal to the sample surface and significantly enhances the signal strength, especially normal to the sample surface.

(III) The plasma regime. At high incident power densities, surface melting and evaporation occur, resulting in material ablation and the formation of plasma above the sample surface. The momentum of the evaporated material exerts an opposite force on the sample, causing a reactive stress at the surface. This generates an intense broadband ultrasonic source, whose strongest components are, directed normal to the surface. In this study, vacuum grease was applied to sample surface to enhance the signal, and ultrasound was thus generated by a combination of I, II and III above.

2.7 METHODS OF INTERFEROMETRY

Interferometers for the detection of ultrasonic movements of waves may be divided into two main types. In the first type, light scattered or reflected from a surface is made to interfere with a reference beam, thus giving a measure of optical phase and hence instantaneous surface displacement. The second type of interferometer makes use of interference between a large number of reflected beams. This is designed as a high-resolution optical spectrometer to detect changes in the frequency of the scattered or reflected light. It thus gives an output dependent on the velocity of the surface. The first type is the more widely used and the most practical at lower frequencies and with reflecting surfaces. The second type offers a potentially higher sensitivity with rough surfaces at higher frequencies.

For the detection of ultrasonic waves at a surface, the techniques are admittedly insensitive compared with piezoelectric devices. They do, however, offer a number of advantages.

- (1) The potential for rapid area scanning, non-contacting (no couplant) generation and no fundamental restriction on surface temperatures.
- (2) High spatial resolution may be obtained without reducing sensitivity; the measurements may be localized over a few micrometers if necessary.
- (3) As the measurements may be directly related to the wavelength of the light, no other calibration is required.
- (4) They can have a flat broadband frequency response, something difficult to achieve with piezoelectric transducers, particularly at high frequencies.

2.8 HE-NE LASER HETERODYNE INTERFEROMETER.

2.8.1 Principle of Detection

The complex amplitude of a laser beam of frequency f_L can be written as:

$$L = e^{2i\pi f_L t}$$

This is divided into a reference beam and a signal beam, whose complex amplitude is:

$$R = r \cdot e^{2i\pi f_L t}$$

The reference beam does not experience any perturbation, however the signal beam experiences a frequency shift f_B in the Bragg cell. Upon reflection on the object, its phase is modulated by the displacement of the sample:

$$\varphi(t) = 4\pi \cdot d(t) / \lambda$$

Where λ is the wavelength of the laser beam and $d(t)$ the mechanical displacement of the object. The complex amplitude of the signal beam is therefore:

$$S = s \cdot e^{2i\pi f_L t + 2i\pi f_B t + i\varphi(t)}$$

The interference of the two beams on the photodetector produces an electrical signal at frequency f_B , phase modulated by the displacement of the object:

$$I(t) = I_0 + I(t)$$

$$I(t) = k \cos(2\pi f_B t + \varphi(t))$$

The useful signal is contained in the signal delivered by the photodetector as a phase modulation of the carrier frequency. The signal processor delivers an electric signal proportional to the displacement of the object. Half of the current $i(t)$ is filtered at the frequency f_B , and phase shifted by 90° . It is then mixed with the other half, non perturbed, and yields a current:

$$j(t) \propto \cos(2\pi f_B t + \varphi(t)) \times \cos(2\pi f_B t + \pi/2)$$

$$j(t) \propto 1/2 [\cos(4\pi f_B t + \varphi(t) + \pi/2) + \cos(\varphi(t) + \pi/2)]$$

The signal at the frequency $2 f_B$ is filtered, to give:

$$s(t) \propto \sin \varphi(t)$$

If the displacement is very small compared to the optical wavelength, this signal can be written as:

$$s(t) = k \cdot 4\pi \cdot d(t) / \lambda$$

The final electrical signal is therefore directly proportional to the displacement of the object.

2.8.2 Working of Heterodyne Interferometer (optics)

The system consists of an optical head. The optical layout is shown in figure 2.1. The laser beam emitted by the laser source is horizontally polarized, is directed in the interferometer by two deflecting mirrors. The laser beam is split into two parts by the beamsplitting cube. The reference beam is reflected by the beamsplitting cube and goes through the Dove prism. It is then transmitted by the polarizing beamsplitting cube and deflected by the mirror on the photodetector. The probe beam is transmitted by the beamsplitting cube and is horizontally polarized. Its optical frequency is shifted in the Bragg cell, and transmitted by the polarizing beamsplitting cube. A quarter wave plate transforms the horizontal polarization into circular polarization. The lens focuses the beam on the surface of the sample.

The probe beam is then phase modulated upon reflection on the sample by the mechanical displacement. After the second pass in the quarter wave plate, the direction of polarization becomes vertical. The probe beam is reflected by the polarizing beamsplitter on the photodetector. Just after the polarizing beamsplitter, the polarization of the probe and reference beam are respectively vertical and horizontal. These two beams can therefore not interfere. The analyzer selects a common component at 45° of the two polarizations, thus allowing interference. The photodetector delivers a beat frequency of the Bragg cell phase modulated by the mechanical displacement of the object.

2.8.3 Sensitivity

Laser ultrasonics suffers from a lack of sensitivity relative to conventional ultrasonics as the photon structure imposes a fundamental limit on the change in light levels during generation / detection of lasers.

Overall sensitivity to flaws is given by:

$$\text{Sensitivity} = T \times f(\sigma, A) \times R$$

Where T , $f(\sigma, A)$, R are terms related to the transmitted sound, the focal or imaging properties of the system determined by the flaw scattering σ and the focal aperture A , and

the receiver sensitivity. The generated signal can be improved using tailored surface coatings or by increasing the power of the generating source. However this approach is limited by the onset of ablation in the target.

2.9 CLOSURE

In this Chapter, the basic theory of generation of ultrasonic waves by lasers and their detection using laser-based interferometers has been presented. Some of the important properties of lasers related to aspects of generation and detection of ultrasonic waves have been discussed. Advantages of using laser based detectors despite poorer detectivity and sensitivity has also been explained.

- 1- Single Frequency He-Ne Laser
- 2- Deflecting Mirrors
- 3- Beamsplitter
- 4- Dove Prism
- 5- Polarising Beamsplitter

- 6- Bragg Cell
- 7- Quarter Wave Plate
- 8- Focussing Lens
- 9- Deflecting Mirror
- 10- Analyser
- 11- Photodetector

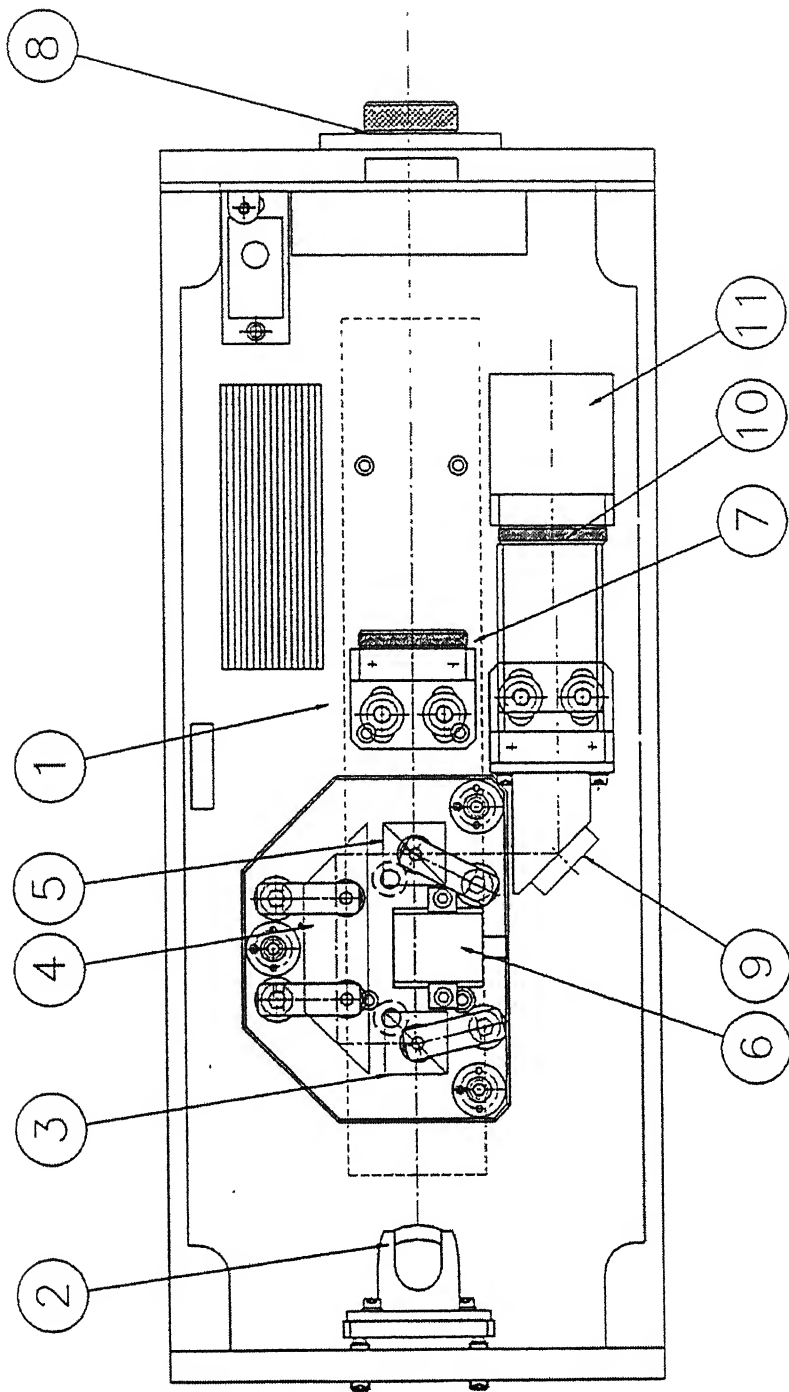


Fig. 2.1 Optical Layout of Heterodyne Interferometer

N° PLAN : 41 123 01/2	DESIGN : CABLE	LE 12/02/73
DESIGNER : S/ENSEMBLE	TRACÉ : LA	CONTRÔLE :
RÉVISION :		01/11/03/05/07/08/09/10/11/12/13/14
CE PLAN NE DOIT ÊTRE EXÉCUTÉ SEULEMENT EN CONCORDANCE AVEC L'INTERPRÉTATION ÉCRITE		

EXPERIMENTAL SET-UP AND PROCEDURE

This Chapter briefly describes the details of laser based ultrasonic setup and the conventional piezoelectric ultrasonic setup and data collection.

3.1 EXPERIMENTAL SETUP: LASER BASED ULTRASONICS

Nd: YAG Pulse Laser is used to generate ultrasonic waves in any media, which is to be inspected. Heterodyne type Laser Interferometer is used to detect the transmitted wave, the signals are then amplified and digitized using a Yokogawa DL1740 digital oscilloscope. The oscilloscope is triggered using a synchronization signal from the pockels cell of the pulsed laser. Recorded waveforms are transferred to a HP Pentium III computer over a USB/Ethernet interface for subsequent storage and analysis which is then captured in a Digital Storage Oscilloscope. The schematic layout of experimental setup is shown in Fig.3.1 and a photograph of the same is shown as Fig. 3.2. The scanning is done manually using 2 single axis micrometer controlled devices mounted on the Optical Test Bench. A brief description of the setup is given in the following paragraphs.

3.1.1 Nd: YAG Pulsed Laser Ultrasonic Generator.

The 5000 DNS series pulsed Nd: YAG laser is built on a modular concept. The optical configuration allows variable setting of the optical parameters. It consists of 3 major components, the laser-head, the power supply and the cooling unit. The heart of the system is the pumping structure, which houses the Nd: YAG rod and the flash lamp. The lasers are built on an electro-optically Q-switched oscillator. This oscillator uses a pockels cell Q-switch to produce pulses of high intensity and short duration (5-7 ns). Q- Switched Lasers are often used as a non-contact ultrasound source in non-destructive testing of materials. Q-switched lasers typically have nanosecond (ns) pulse durations and generate broadband ultrasound waves, though longer laser pulses, of 100 microseconds or greater, have been used for NDE. A variable reflectivity output coupler allows the extraction of high energy on a single spatial transverse mode. This leads to laser beams of low divergence, and to high conversion

efficiencies in the harmonic wavelengths (1064, 532, 355, 266 nm). Different harmonic generators extend the wavelength range to the second, third and fourth harmonics.

The active medium of the laser operates on transitions of triply ionized Neodymium atoms (Nd^{3+}), which take place of another ion (Yttrium) in the host: Yttrium Aluminum Garnet known by the acronym YAG. The laser operates as a 4-level system. The intense broad-spectrum light of the flash lamp populates the upper level. Once in the higher energy level, the Neodymium ions drop to a metastable level, producing a population inversion. The lower level decays by a fast non-radiative process to the ground state. The strongest Neodymium line is 1064 nm.

3.1.2 Optical Heterodyne Laser (He-Ne) Probe.

The SH-130 probe is designed to measure transient mechanical displacements of very low amplitude. It is specially devoted to measuring displacements generated by the propagation of an acoustic or ultrasonic wave. The system consists of a compact optical head and an electronic signal-processing unit. The optical head integrates high stability, low power laser source for fast detection with a high spatial resolution.

The electronic signal processor delivers a response proportional to the displacement of the target, with a high bandwidth. The output signal is automatically calibrated to give the absolute value of the measured displacement. The principle of detection (heterodyne interferometry) makes the system insensitive to external vibrations. The compactness of the system allows for a wide range of operating conditions.

3.1.3 Digital Storage Oscilloscope

The setup utilizes a Yokogawa DL1740 (four channel, one GSa/sec, 500 MHz) Digital Storage Oscilloscope, having built in Zip drive, Ethernet, USB, GPIB and Serial Ports for communication with external PC's/ systems.

3.1.4 Computer

The DSO is interfaced to a Pentium III based PC and Data is stored on-line using communication through USB and Ethernet ports.

3.2 EXPERIMENTAL PROCEDURE (LBU)

3.2.1 Installation And Calibration Of Setup.

The calibration of the optical probe involved the following procedural steps:

- (1) Mounting of Test Specimen. All tests were carried out on a piezo-electric ceramic specimen prepared with one side having an extremely high reflective surface. The source and receiver are aligned on opposite sides of a parallel-sided sample.
- (2) Alignment of the SH-130 Optical Probe. This involved optimizing the control signal by adjusting the orientation of the sample, and fine-adjustment of its distance from the focusing lens. (The focal length of the focusing lens is around 215 mm.)
- (3) The photo detector output was measured without going through the signal processor. This was found to be 310 mV (As per specifications). Print out of the DSO image is placed at Appendix 'A'.
- (4) The output was then taken through the signal processor with the automatic gain control switched on. The measured signal was found to be in excess of the stipulated signal level of 630 mV peak to peak on 50 Ω . (Found to be 730 mV.) This was adjusted using the adjustments available in the signal-processing unit. Print out of the DSO image is placed at Appendix 'B'.
- (5) Sensitivity: A sinusoidal voltage, of frequency higher than 200 kHz, (263 kHz) was applied to the sample. The non-demodulated signal was taken into a separate channel of the DSO and spectrum analysis was carried out using Matlab. The demodulated signal was taken to another channel of the DSO. The voltage applied to the sample was adjusted so that the ratio between the carrier at 70 MHz and the sideband at 70 MHz +>200 KHz is 40 dB, which corresponds to a displacement of 10 A° amplitude. The corresponding voltage was measured on the Oscilloscope and the calibration factor was calculated. The accuracy of the measurement was within the stipulated ten percent limits. The measured sensitivity was 10 mV/ A°. Print out of the DSO image is placed at Appendix 'C'.
- (6) Detectivity: To ascertain the detectivity, voltage applied to the sample was decreased until the signal to noise was equal to one. This was visually ascertained

on the DSO as laid down in the technical manual. The measured displacement was determined and the detectivity was calculated. The measurement was repeated for each standard bandwidth (4,18 and 45 MHz). The measured detectivity was found to be higher than that recorded at the manufacturers facility, this was primarily due to additional focusing and signal collection arrangements at the input of the optical probe available with them. The detectivity however was found to be within requirements of the existing setup. Print out of the DSO images is placed at Appendix 'D'.

3.2.2 Preparation Of Specimen

The present ultrasonic nondestructive evaluation is done on composite specimens implanted with artificial inclusions like Teflon insert and Resin rich zones. The specimens are prepared by hand lay up technique, using woven glass fabric (24 plies) as the reinforcing material and epoxy resin as the matrix material. Resin used being LY556, hardener HT976 and accelerator XY73 all manufactured by Ciba Geigy (India). The curing was done at 120° C and 5 Atm pressure for one hour followed by one hour at 150° C and 5 Atm pressure and left to cool to room temperature at same pressure overnight.

The dimensions of the finished specimens were 60 x 60mm². Model specimens were prepared with a central Teflon insert to simulate delamination. The Teflon inserts, circular in shape, 15mm in diameter and about 0.5mm in thickness was introduced centrally in the thickness direction (in between plies 12 and 13). The specimen with resin rich zone had square cutouts of 15mm X 15mm in central 8 plies (Ply No. 9 to 16). During casting, this region was filled up with resin leaving a resin rich zone in the final laminate. All the specimens were cast with sixteen plies with a final thickness of around 3 mm.

3.2.3 Scanning Procedure

The specimen is cleaned and the area under investigation is marked. The Nd:YAG laser is focused onto the specimen using an arrangement of optical mirrors and lenses (as shown in figure 3.1) so that it acts as a point source and is perpendicular to the irradiated face of the specimen. The power level of the laser is adjusted so that there was minimum ablation of the specimen. The scanning is performed at setting

corresponding to 1064nm wavelength for the Nd: YAG laser. The He-Ne laser is focused on the opposite side of the specimen at the focal length of the collection lens (approx 215mm). The output of the Optical probe was fed to the electronic signal-processing unit. The electronic signal processor delivers a response proportional to the displacement of the target, with a high bandwidth. The output signal is automatically calibrated to give the absolute value of the measured displacement. This is fed to the DSO where it is displayed and storage of the data is carried out on line in the PC interfaced to the DSO.

3.3 PIEZOELECTRIC ULTRASONIC SETUP

The schematic diagram of conventional ultrasonic automated scanning setup, to perform A-scan is shown Fig.3.3. The present ultrasonic experimental setup, developed in-house, consists of scanning tank, a high resolution type Ultrasonic Flaw Detector (UFD), a high speed data acquisition and other accessories for precision movements of the transducers, data collection and storage. A brief description about the setup is given in the following paragraphs.

3.3.1 Scanning Tank

The purpose of the scanning tank is to house the stepper motors, the probes and the specimen. As is common practice, the probes and specimens are immersed in water, which acts as a coupling medium. The tank is made up of Perspex sheets. Two lead screws, each having pitch of 4 mm, have been fixed in mutually perpendicular directions on a frame located at the top of the tank. The probes mounted on the lead screw could be moved in x-y plane with a step of 1 mm in either direction.

3.3.2 Ultrasonic Flaw Detector

The Ultrasonic Flaw Detector (UFD) (Krautkammer-Branson make, USIP12) is used for generating and collecting the ultrasonic signal with the help of probes. The UFD can be used with a single probe in pulse-echo transmission method or with two probes in through-transmission method. The received signal can be obtained from UFD in rectified or radio frequency (RF) mode. There are four controls (for Gain adjustment) by means of which the gain of the received signal can be adjusted to the desired level to reduce noise and avoid any saturation. Various controls are provided for fine

adjustments of frequency range, echo shape, pulse repetition frequency, Distance Amplitude Correction (DAC), Monitor adjustment, back wall echo.

3.3.3 Computer

A microcomputer (PC-AT 386SX) is used to control the stepper motors, UFD, A/D converter for data collection and storage.

3.3.4 Stepper Motor And Controller

The stepper motor (STM 601 with 12v input) of torque capacity 2kg-cm with maximum step rate of 1023 steps/sec were used. The motor can be moved either clock-wise or anti-clockwise direction through stepper motor control card PCL-211 (manufactured by Dynalog Microsystems). In the present setup, motors are moved with 50 clock pulses at a time, which corresponds to 1 mm linear movement of the probe.

3.3.5 Analog To Digital Converter

SONTEK STR* 8100 A/D board is used to digitize RF signal from UFD with a maximum data acquisition flexibility through a 64k on-board high-speed memory buffer. The various board functions, under software control, are input channel selection AC/DC coupling, input voltage range, RF/Video mode, sampling rates, trigger selection, clock control, threshold phase and level, board selection and interrupt enabling. The board's high-speed data acquisition memory is mapped directly into PC memory space. Once the waveform has been captured, the PC can transfer data off the board at 1.5 MHz rate (8 bit) or 3 MHz rate (16 bit) using simple memory block instructions. This board provides freedom from the static architecture of a stand alone instrument and the computer. The D100A Digital Oscilloscope is used to examine the waveform for selecting the appropriate scan parameters such as delay, gate start, gate length etc. In the present setup the A/D board is installed outside the PC using the PCX-795 PC XT/AT bus expansion system. This board has on-board 1,2,4,8,16 and 32 wait state generation, switch setting for memory bank selection, switch setting for I/O selection and switch setting for DMA channel selection.

3.3.6 Transducers

The transducers (probes) used in the present investigation are Immersion Straight Beam probes Z10M, which generate broadband longitudinal waves. They are connected to the UFD by waterproof connectors. The fixtures were fabricated to hold the transducers in vertical position.

Immersion probes are mainly applied for mechanized or automatic ultrasonic test. In principle they work same as contact probes. A major part of the tests is made in immersion tests tanks filled with water. The diameter of the transducer element is 5 mm (element size). The size of the element strongly affects the shape of the transmitted sound field. The probe has nominal frequency of 10MHz. The frequency has a great influence on the evaluation of reflectors with increasing frequency, the echo height from non-vertically positioned reflectors to the sound beam decreases.

3.4 EXPERIMENTAL PROCEDURE

In the present work, the specimens tested were the same as those used for testing using the LBU setup. The specimen to be investigated is cleaned and area under investigation is marked. Then, the specimen is positioned between the Transmitter and Receiver. Probes are brought to the starting position by moving the motor. The gap between the specimen plate surface and the probe surface are adjusted, so as to distinctly observe the initial burst on the UFD oscilloscope screen. The gain adjustment controls are so adjusted that the peak of the signal does not exceed 80% of the maximum screen height of the UFD to avoid saturation. The RF signals from UFD can be also viewed on the digital oscilloscope provided by the software of the A/D board. The gate parameters on the signal to be digitized are made in data file. In these experiments, the data collection is in one dimension only.

A master control code (in C-language) developed for the present investigation controls precise movements of stepper motors and controls the A/D card to collect received waveform in the digitized form. The code is also capable to extract different time and frequency domain features of the waveform during scanning. The initial settings, such as channels, AC/DC coupling, clock source (Intern/Extern), sampling rate (100/200/300/400), trigger type (off/on), post trigger delay, buffer start, buffer length, horizontal delay, gate start, gate length, xfer type (8/16) are set in a data file prior to the execution of the code.

3.5 CLOSURE

In this Chapter the details of experimental setup and procedure were presented both for the Laser Based Ultrasonics setup and the existing water immersed conventional contact ultrasonic system. Experimental procedure for data acquisition was also explained.

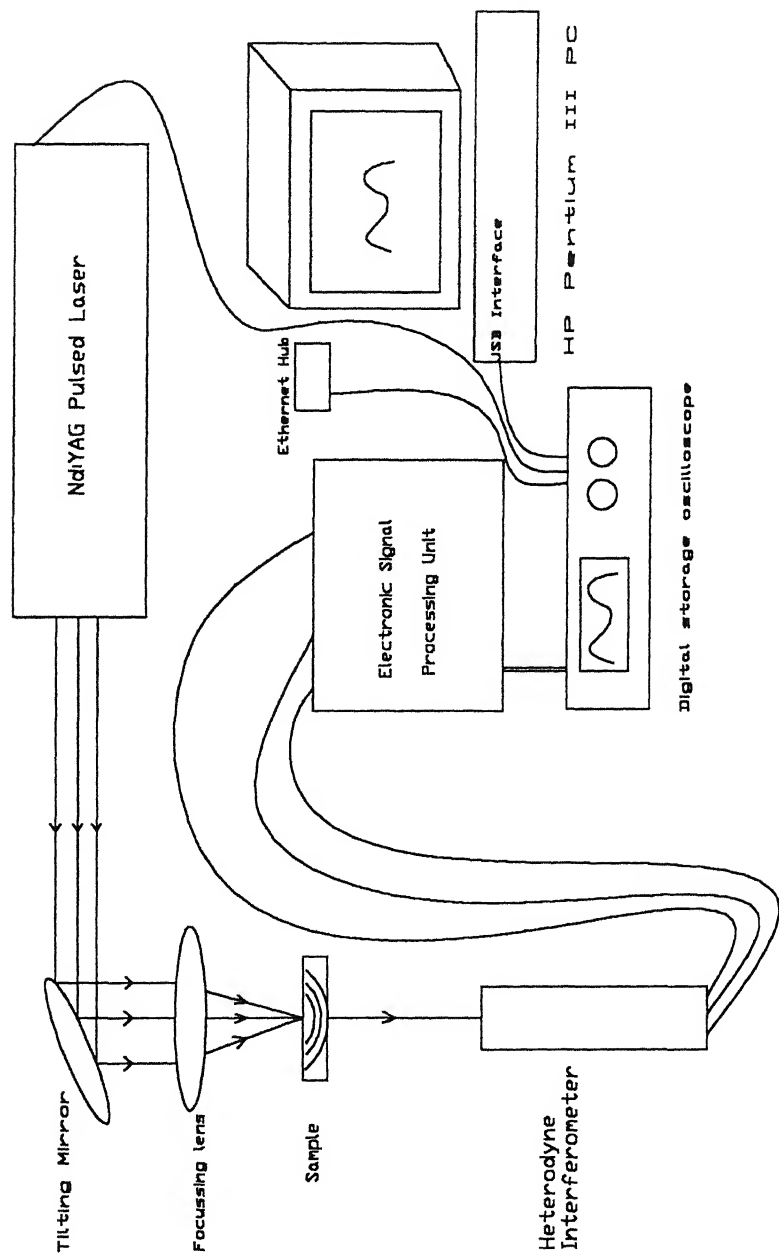


Fig 3.1 Schematic diagram of the experimental setup.

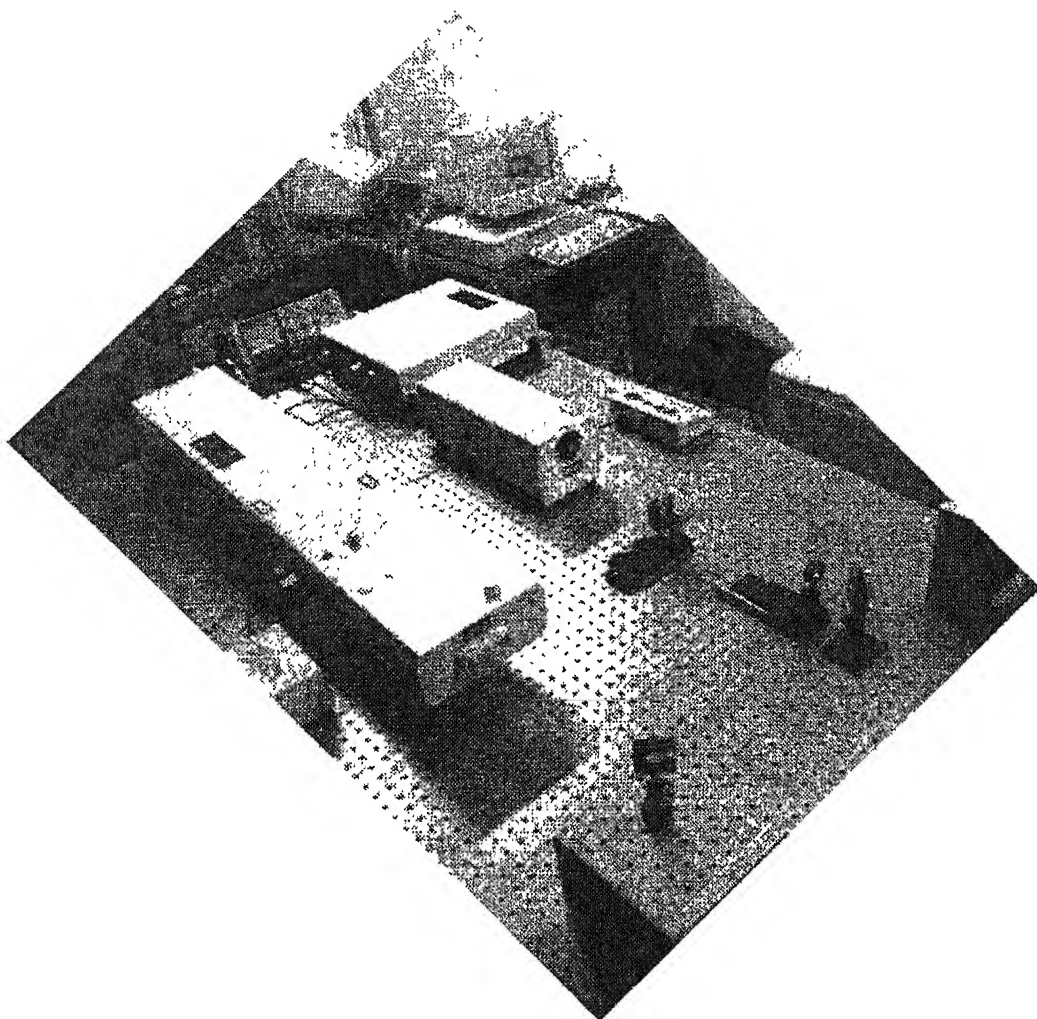


Fig. 3.2 Photograph of Experimental setup (LBU)

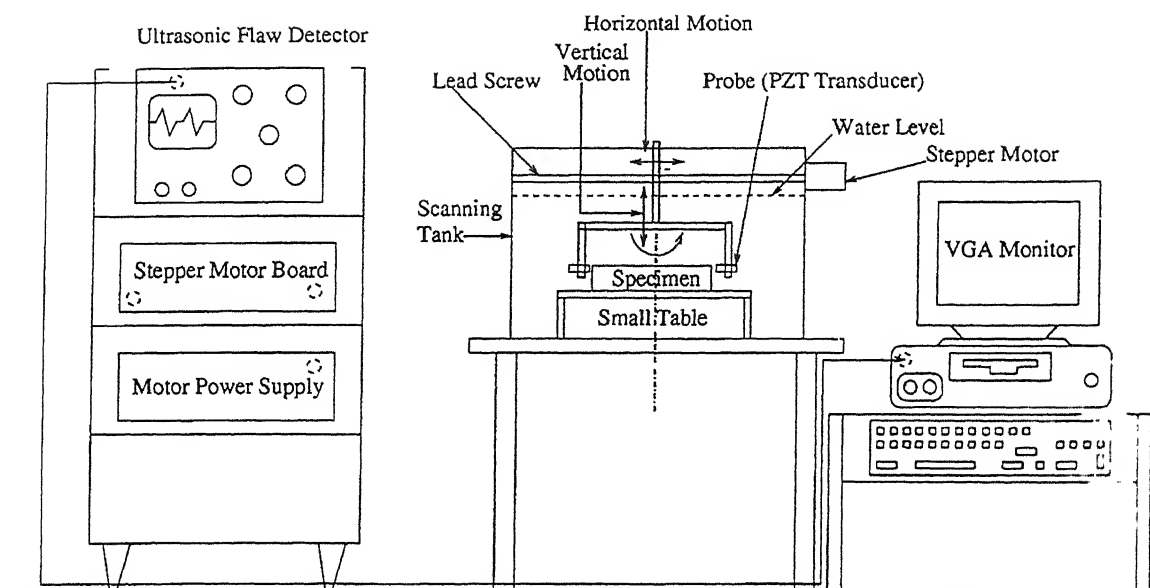


Fig 3.3 Schematic layout of Experimental setup (Conventional Ultrasonics) .

BASICS OF SIGNAL PROCESSING, WAVELETS AND CLUSTER ANALYSIS

4.1 INTRODUCTION

Composites may contain many types of damage modes, such as delamination, debonding, resin richness, fiber breaks, matrix cracking etc. either individually or in combinations. The variations in the type of flaw, local heterogeneity in the composite materials and other instabilities, cause statistical variation in the signal. To identify a particular damage type, specific information in the form of features, must be extracted from the signal [2]. Each type of damage interacts with the signal in a unique way causing certain changes in the relevant features of it. These variations must be detected and quantified for being used in the identification process. In relation to ultrasonics, peak amplitude, time of flight, rise time, pulse duration, fall time, may be some of the time domain features and amplitude of different frequency components or harmonics, phase values may be the frequency domain features. In the present study, a decision algorithm developed using cluster analysis, to evaluate the usefulness of frequency domain features in detecting delaminations and resin rich zones developed by Datta [4], has been used. This exercise has been carried out for data generated by scanning defective samples by both LBU and conventional ultrasonics setup.

The Non Destructive Testing aims to have the highest possible probability of detection, the most exact size and the exact orientation of defects. The possibility to acquire some information to characterize defects in nature, size and orientation has necessitated the development of techniques more evolved than those that are regrouped under the general technical term of ultrasonic imaging. In the present work an algorithm has been used based on wavelets transform in order to enhance flaw visibility. Wavelet transforms have generated much interest in various applications such as speech coding, pitch detection, image compression, multiresolution analysis and estimation of multiscale

processes. The idea of examining signals at various scales and analyzing them with various resolutions has, in fact, emerged independently in many fields of mathematics, physics and engineering. Wavelet decomposition introduces the notion of scale as an alternative to frequency and maps a signal into a time-scale plane. Each scale in the time-scale plane corresponds to a certain range of frequencies in the time-frequency plane. By combining the time domain and the classical Fourier analysis, the wavelet transform provides simultaneous spectral representation and temporal order of the signal decomposition components. Construction of a C-scan image from A-scan signals has been implemented by a selection process of wavelet coefficients, followed by an interpretation procedure in the time-frequency domain.

4.2 DIGITAL SIGNAL PROCESSING

Digital Signal Processing (DSP) concepts were introduced many years ago and later emerged as the primary means of detecting, conditioning and automatically classifying a variety of signal types. Unfortunately Ultrasonic Nondestructive Evaluation (UNDE) and UNDE Instrumentation Development have not exploited the advantages offered by DSP implementations as much as one would expect. This is in spite of the fact that compared to analog signal processing systems; digital systems have the following advantages:

1. Greater Signal Transmission Fidelity
2. Large Non-volatile Storage capabilities
3. Processing/calculation/classification capabilities, and
4. More sophisticated filtering and signal analysis methods

4.2.1 Digitizing the Time Axis

A continuous time analog signal $x_a(t)$ has to be converted into a sequence of discrete time signals, represented by a sequence of numbers x , denoted $x[n]$, with n being the n^{th} number in the sequence. Such a sequence is the result of periodic sampling of the continuous time analog signal $x_a(t)$,

$$x[n] = x_a(nT)$$

T is the sampling period, and $1/T$ the sampling rate or sampling frequency. For ultrasonic applications this is typically in the MHz range. The sampling frequency, $\Omega_S = (1/T)$, has to be greater than the bandwidth Ω_N of the signal being sampled. More precisely, according to the Nyquist Sampling Theorem, for a correct representation of a digitized signal, the sampling frequency Ω_S has to be at least twice as high as the bandwidth Ω_N :

$$\Omega_S = 2\pi/T > \Omega_N$$

Under-sampling, or sampling at rates less than the Nyquist requirement will cause "aliasing", which results in "shadow frequency images" of the original signal.

4.2.2 Digitizing Signal Amplitude

The A/D converter performs the initial amplitude discretization for the input analog ultrasonic signal prior to further conversion needed during processing by either a fixed or floating-point signal processor. This conversion process quantizes the signal amplitudes into a sequence of finite-precision samples. The precision or quantization error is determined by the number of amplitude quantization levels. This quantization error can be represented as an additional noise signal component.

4.2.3. Time and frequency

Fourier analysis is well known technique of signal processing, which breaks down the signal into constituent sinusoids of different frequencies. The *Fourier Transform* (FT) is a technique to transform time-domain signal $f(t)$ into frequency- domain signal $F(\omega)$. Fig.4.1 shows an example of the *Fourier Transform*. Mathematically the *Fourier Transform* is given by

$$F(\omega) = \int_{-\infty}^{\infty} f(t).e^{-i\omega t} .dt$$

and its inverse,

$$f(t) = \int_{-\infty}^{\infty} F(\omega).e^{i\omega t} .d\omega$$

where, ω is the frequency. In *Fourier Transform*, the main drawback is that the time

information is hidden. When looking at a FT of a signal, it cannot be seen when the particular spectral components appear exactly in the signal.

4.2.4 SHORT TIME FOURIER ANALYSIS (STFA)

Short-Time Fourier Transform (STFT) is a modification of the Fourier transform. STFT has adapted by *Dennis Gabor* (1946), to analyze a small section of the signal at a time, a technique is called *windowing* a signal. Fig. 4.2(a) shows transformation of a signal into two-dimensional function of time and frequency. Mathematically the STFT, with window function $w(t-\tau)$ is expressed as

$$STFT(\omega) = \int_{-\infty}^{\infty} f(t).w(t-\tau).e^{i\omega\tau}.dt$$

where, $w(t-\tau)$ is the analysis filter or analysis window. The STFT represents a compromise between the time-domain and frequency-domain views of a signal. It provides information about frequency content in the window of the signal at the given time. However, this information is obtained with limited precision, and that precision is determined by the size of the window. The drawback is that once a particular size is chosen for the time window, that window is the same for all frequencies. Many signals require a more flexible approach, where the window size can vary to determine more accurately in either time-domain or frequency-domain.

4.3 WAVELET ANALYSIS (WA)

Wavelet Analysis is the next logical step in which the windowing technique with variable sized regions is used. Wavelet analysis allows both low frequency information with long time intervals and high frequency information with shorter regions. Fig. 4.2(b) shows that wavelet analysis does not use a time-frequency region, but rather a time-scale region. Mathematically, the *Wavelet Transform* (WT) of a signal is defined as follows: (Legendre et al [15])

information is hidden. When looking at a FT of a signal, it cannot be seen when the particular spectral components appear exactly in the signal.

4.2.4 SHORT TIME FOURIER ANALYSIS (STFA)

Short-Time Fourier Transform (STFT) is a modification of the Fourier transform. STFT has adapted by *Dennis Gabor* (1946), to analyze a small section of the signal at a time, a technique is called *windowing* a signal. Fig. 4.2(a) shows transformation of a signal into two-dimensional function of time and frequency. Mathematically the STFT, with window function $w(t-\tau)$ is expressed as

$$STFT(\omega) = \int_{-\infty}^{\infty} f(t).w(t-\tau).e^{i\omega\tau}.dt$$

where, $w(t-\tau)$ is the analysis filter or analysis window. The STFT represents a compromise between the time-domain and frequency-domain views of a signal. It provides information about frequency content in the window of the signal at the given time. However, this information is obtained with limited precision, and that precision is determined by the size of the window. The drawback is that once a particular size is chosen for the time window, that window is the same for all frequencies. Many signals require a more flexible approach, where the window size can vary to determine more accurately in either time-domain or frequency-domain.

4.3 WAVELET ANALYSIS (WA)

Wavelet Analysis is the next logical step in which the windowing technique with variable sized regions is used. Wavelet analysis allows both low frequency information with long time intervals and high frequency information with shorter regions. Fig. 4.2(b) shows that wavelet analysis does not use a time-frequency region, but rather a time-scale region. Mathematically, the *Wavelet Transform* (WT) of a signal is defined as follows: (Legendre et al [15])

$$W_f(a, b) = \int_{-\infty}^{\infty} f(t) \cdot \frac{1}{\sqrt{a}} \psi\left(\frac{t-b}{a}\right) dt$$

where, $\psi(t)$ is a mother wavelet, b is a time shift parameter and a is a scaling parameter.

By definition, the WT is the correlation between the signal and set of basic *Wavelets*.

Wavelet analysis produces a time-scale view of a signal, with scaling and shifting.

Scaling a *Wavelet* means stretching (or compressing) it. Fig. 4.3 shows wavelets with different scaling parameters. Shifting a Wavelet simply means delaying (or hastening) its onset. Mathematically, delaying a function $f(t)$ by τ is represented by $f(t - \tau)$. Fig. 4.4 shows wavelets with different shift factors.

Wavelet analysis is capable of revealing aspects of data that other signal analysis techniques miss such as trends; break down points, discontinuities in the higher derivatives and self-similarity. Wavelet analysis can *compress* or *de-noise* a signal without appreciable degradation.

Wavelet analysis can be performed in two ways

1. Using continuously translated and dilated versions of mother wavelet (CWT), or
2. Using discretely translated and dilated versions of mother wavelet (DWT).

4.3.1 Continuous Wavelet Transform (CWT)

The continuous wavelet transform (CWT) is defined as the sum over all time of the signal multiplied by scaled and shifted versions of the wavelet function ψ , which can be represented as

$$C(a, b) = \int_{-\infty}^{\infty} f(t) \psi_{a,b}^*(t) dt$$

Where, $C(a, b)$ are the coefficients of the wavelet transform, $f(t)$ is the signal being analyzed and $*$ denotes the complex conjugate of $\psi_{a,b}$. Here, $\psi_{a,b}$ is the shifted and scaled version of the mother wavelet $\psi(t)$ as given by,

$$\psi_{a,b} = a^{-1/2} \psi\left(\frac{t-a}{b}\right), (a,b) \in \mathbb{R}^2, a > 0$$

The word continuous in CWT means, that the transform operates the wavelets on the signal with continuous in scaling and shifting. During the computation, the analyzing wavelet is shifted smoothly over the full domain of the analyzed signal/function.

4.3.2 Discrete Wavelet Transform (DWT)

Calculating Wavelet coefficients in CWT at every possible scale generates a very large amount of data. This disadvantage of CWT is overcome by choosing scales and positions based on powers of two, so called dyadic scales and position, which is more efficient and just as accurate. Such an analysis is called Discrete Wavelet Transform (DWT). The generation of the wavelets and calculation of the DWT are well matched to digital computer. The wavelet transform can also be expressed in discrete form

$$f(t) = A \sum_m \sum_n C_{m,n} \psi\left(\frac{t - na_0^m T}{a_0^m}\right)$$

where,

$$C_{m,n} = a_0^{-m/2} \int f(t) \psi\left(\frac{t - na_0^m T}{a_0^m}\right) dt$$

$$a = a_0^m$$

$$b = na_0^m T$$

where, T is the sampling period, A and a_0 are constants, where $a_0=2$ for the dyadic wavelet transform, m is depend upon the number of decomposition levels and n is depend upon the length of the signal to be decomposed.

4.3.3 Multi Resolution Analysis (MRA)

Multi resolution wavelet analysis allows the decomposition of a function/signal in progression of successive *approximation* and *details*, corresponding to different scales. The *approximations* are high-scale, low frequency components and the *details* are the

low-scale, high frequency components of the signal. The difference between the actual signal and its approximation of order n is called its *residual*. Intuitively, the *approximation* is relatively smooth, and *detail* being composed of high frequency components. The *detail* corresponds to the difference between two successive levels of approximation.

4.3.4 Multiple-Level Decomposition

In DWT, the decomposition process can be iterated, with successive approximations being decomposed in turn, so that one signal can be broken into many lower-resolution components. This is called the *Wavelet decomposition tree*. Fig. 4.5 shows the Multi-level (three level) wavelet decomposition tree.

4.3.5 Wavelet Reconstruction

Wavelet reconstruction, or *synthesis* is the process of reconstructing the decomposed signal using a set of decomposed coefficients. The mathematical manipulation that affects synthesis is called the *inverse discrete wavelet transform* (IDWT).

4.3.6 Properties of Wavelets

The best-performing *mother wavelet* should have the following three properties.

1. The admissible condition is given by

$$\int_{-\infty}^{\infty} \psi(t) dt = 0$$

2. The wavelet has the characteristic of good time-frequency localization. This property makes the wavelet transform is powerful tool for analysis of non-stationary signals such as sound, seismic, electromagnetic signals etc.

3. The power spectrum of the wavelet is well matched with that of the signal to be analyzed.

4.3.7 Different types of Wavelets

A wavelet is a waveform of limited duration, which has the above properties. Different types of mother wavelets are discussed in the following paragraphs.

The simplest wavelet is *Haar* wavelet, which is a step function (Figs. 4.6(a) and 4.6(b)). Ingrid *Daubechies*, invented what are called compactly supported orthonormal wavelets. The names of the *Daubechies* family wavelets are written as *dbN*, where N is the order, and *db* is the “surname” of the wavelet. The *db1* wavelet is same as *Haar*. Figs. 4.6(c) through 4.6(p) shows the scaling and wavelet functions of the various *Daubechies* wavelets. In *Biorthogonal* wavelets two types of wavelet functions are used: one for decomposition and other for reconstruction instead of the same one. *Coiflets*, *Symlets*, *Morlet*, *Mexican Hat*, *Mayer* etc. are other different type of wavelets suitable for various purposes.

There are different wavelets that can be used to decompose the signal and extract feature vector. These wavelets include *Daubechies* (*db1*-*db10*), *Biorthogonal* (*bior1.3*-*bior6.8*), *symlets* (*sym2*-*sym8*), *coiflets* (*coif1*-*coif5*), *Morlet*, *Mexican hat* and *Meyer*. The criterion for selection of the proper mother wavelet is based on the shape of the wavelet function, which could match well with the shape of the signal mode to be analyzed. In the present work, *Coiflets*, order 5 (*coif5*) has been chosen, because it seems to match with the signal mode to be analyzed and also it possesses good time-frequency localization. Figs. 4.6(a) to 4.6(q) shows different type of wavelet and scaling functions. Fig. 4.6(q) shows the *Coiflets*-1 to 5 (*coif5* has been used in the present work.)

4.4 NOISE SUPPRESSION

In Ultrasonic Nondestructive Evaluation (NDE), the observed ultrasonic signal $S(t)$ can be expressed as the sum of the two components.

$$s(t) = y(t) + n(t)$$

where, $y(t)$ is the signal of the defect and $n(t)$ is the noise. Noise removal is extremely important in the ultrasonic defect detection to identify the defects correctly. Optimal de-noising requires a more subtle approach called thresholding. This involves discarding only the portion of the details that exceeds a certain limit.

The main steps of the signal noise removal are.

1. Decomposition of the signal into coefficients,
2. Separation of the *approximation* and *detail* coefficients from the coefficients, and
3. Reconstruction of the de-noised signal from the *approximation* coefficients and their different levels of the noises from the *detail* coefficients.

A code for the noise suppression from the signal is available in Matlab GUI. This gives the user options for variable Thresholding, like, fixed thresholding, heuristic sure, rigorous sure, mini-max, penalize high, penalize medium, penalize low. It also facilitates selection of noise structure to be removed, i.e., unscaled white noise, scaled white noise and non-white noise. The signal received in our case from laser as well as conventional ultrasonic setups was found to have unscaled white noise, this option was used alongwith fixed thresholding facility available in GUI of Wavelet toolbox in Matlab and all signals were de-noised before compression.

4.5 DATA COMPRESSION

Compression is one of the most important applications of wavelets. The ability of data compression of the wavelet transform allows one to use a restricted number of wavelet coefficients and possibly a restricted number of wavelet levels to characterise each component of an A-scan ultrasonic signal. Two important assumptions allow us to limit the number of wavelet coefficients and wavelet levels to be considered during the feature extraction step:

- (1) In a recorded signal, one can consider the highest frequency components formed from the first wavelet levels, as representing the noise-not

necessarily the structural noise. As a result, wavelet coefficients contained in them can be ignored.

- (2) The wavelet coefficients contained in the last wavelet levels representing the lowest frequency components of the signal are not significant in our analysis method. Such an assumption is allowed by considering that the following analysis and image generation steps are done in the time-frequency domain and do not require any inverse wavelet transformation.

In the wavelet representation of a signal, Wf , the simplifications induced by taking both of these assumptions into account are done by a procedure of wavelet levels elimination. If H and L are used to represent the thresholds used to eliminate the non significant wavelet levels, only levels at the scale 2^j for $H \leq j \leq L$ are kept. Applying the following procedure modifies the vector d_j (where d_j represents the approximation of $f(n)$ ($f(n)$ is the digitized sequence of signal $f(t)$) at the scale 2^j). The thresholds depend on the reflection and sampling frequencies, and are determined empirically by visual examination of the wavelet decomposition levels. Now,

$$d_j(k) = \begin{cases} 0 & \text{if } j < \tilde{H} \\ d_j(k) & \text{if } H \leq j \leq L \text{ for } k=1, \dots, N/2^j \\ 0 & \text{if } j > L \end{cases}$$

For $j = 1, \dots, J$ and

$$\widehat{W}f = \left[0 \ \widehat{d}_J^T \widehat{d}_{J-1}^T \dots \widehat{d}_j^T \dots \widehat{d}_2^T \widehat{d}_1^T \right]^T, \quad \dim(\widehat{W}f) = N$$

Here Wf is the vectorial wavelet representation of $f(n)$ consisting of a concatenation of all wavelet levels.

It is assumed that the signal features consist of a limited number of highest modulus wavelet coefficients within each retained level. Thus, a simple selection procedure that

sets to zero the wavelet coefficients that are not taken into account completes the preponderant coefficient extraction step. The algorithm written in Matlab for this is placed at Appendix 5.

4.5.1 C- scan image generation

Once the feature extraction procedure has been applied on an A-scan signal, sets of some non-zero wavelet coefficients belonging to one or several wavelet levels d_j at the scale 2^j for $H \leq j \leq L$ are created. These coefficients translate the different components of the analysed signal in the time-frequency domain by parting the frequencies in separate bandwidths while keeping their temporal order. The coherent information in the signal would include that of the defective region in the through scan mode. To extract this information, this feature has to be quantified; this corresponding value is called the characterisation parameter. The characterization parameter propounded by Legendre et al[15] is used. This would establish efficacy of trying to capture signal modification due to presence of defect in through transmission as against capturing flaw reflection by windowing technique as proposed in the paper referred above.

4.6 BASICS OF CLUSTER ANALYSIS

Classification is a process of assigning any item or observation to its proper place in an established set of categories. In fact, cluster analysis is not as much a typical statistical test as it is a "collection" of different algorithms that "put objects into clusters." The point here is that, unlike many other statistical procedures, cluster analysis methods are mostly used when no a priori hypotheses is available, but the research is still in the exploratory phase. In a sense, cluster analysis finds the "most significant solution possible." Clustering methods could be either hierarchical or nonhierarchical. In hierarchical clustering, the sequence of forming clusters proceeds in such a way that whenever two samples are put into one cluster at some stage, they remain together at all subsequent levels. In the nonhierarchical method, initial seed points are selected and the cluster memberships are altered with respect to certain criterion, before the final clusters are obtained. Some of the terms of cluster analysis are explained below (reference [4]).

4.6.1 Hierarchical Tree

Consider a Horizontal Hierarchical Tree Plot (see Fig 4.7), on the left of the plot; to begin with each object is considered as a class by itself. Next, in very small steps, the criterion as to what is and is not unique is relaxed. Put another way, the threshold regarding the decision when to declare two or more objects to be members of the same cluster is relaxed.

By this process more and more objects are linked together and aggregated (*amalgamated*) to form larger and larger clusters of increasingly dissimilar elements. Finally, in the last step, all objects are joined together. In these plots, the horizontal axis denotes the linkage distance (in *Vertical Icicle Plots*, the vertical axis denotes the linkage distance). Thus, for each node in the graph (where a new cluster is formed) the criterion distance at which the respective elements were linked together into a new single cluster can be ascertained. When the data contains a clear "structure" in terms of clusters of objects that are similar to each other, then this structure will often be reflected in the hierarchical tree as distinct branches. As the result of a successful analysis with the joining method, one is able to detect clusters (branches) and interpret those branches.

4.6.2 Distance Measures

The joining or tree clustering method uses the dissimilarities or distances between objects when forming the clusters. These distances can be based on a single dimension or multiple dimensions. The most straightforward way of computing distances between objects in a multi-dimensional space is to compute Euclidean distances. In a two- or three-dimensional space this measure is the actual geometric distance between objects in the space (i.e., as if measured with a ruler). However, the joining algorithm does not "care" whether the distances that are "fed" to it are actual real distances, or some other derived measure of distance that is more meaningful to the researcher; and it is up to the researcher to select the right method for his/her specific application.

4.6.2.1 Euclidean distance

This is probably the most commonly chosen type of distance. It simply is the geometric distance in the multidimensional space. It is computed as:

$$\text{Distance}(\mathbf{x}, \mathbf{y}) = \{\sum_i (\mathbf{x}_i - \mathbf{y}_i)^2\}^{1/2}$$

Note that Euclidean (and squared Euclidean) distances are usually computed from raw data, and not from standardized data. This method has certain advantages (e.g., the distance between any two objects is not affected by the addition of new objects to the analysis, which may be outliers). However, the distances can be greatly affected by differences in scale among the dimensions from which the distances are computed. For example, if one of the dimensions denotes a measured length in centimeters, and this is converted into millimeters (by multiplying the values by 10), the resulting Euclidean or squared Euclidean distances (computed from multiple dimensions) can be greatly affected, and consequently, the results of cluster analyses may be very different.

4.6.2.2 Squared Euclidean distance

One may want to square the standard Euclidean distance in order to place progressively greater weight on objects that are further apart. This distance is computed as (see also the note in the previous paragraph):

$$\text{Distance}(\mathbf{x}, \mathbf{y}) = \sum_i (\mathbf{x}_i - \mathbf{y}_i)^2$$

4.6.2.3 City-block (Manhattan) distance

This distance is simply the average difference across dimensions. In most cases, this distance measure yields results similar to the simple Euclidean distance. However, note that in this measure, the effect of single large differences (outliers) is dampened (since they are not squared). The city-block distance is computed as:

$$\text{Distance}(\mathbf{x}, \mathbf{y}) = \sum_i |\mathbf{x}_i - \mathbf{y}_i|$$

4.6.2.4 Chebychev distance

This distance measure may be appropriate in cases when one wants to define two objects as "different" if they are different on any one of the dimensions. The Chebychev distance is computed as:

$$\text{Distance}(x,y) = \text{Maximum}|x_i - y_i|$$

4.6.2.5 Power distance

Sometimes one may want to increase or decrease the progressive weight that is placed on dimensions on which the respective objects are very different. This can be accomplished via the *power distance*. The power distance is computed as:

$$\text{Distance}(x,y) = (\sum_i |x_i - y_i|^p)^{1/r}$$

where r and p are user-defined parameters. A few example calculations may demonstrate how this measure "behaves." Parameter p controls the progressive weight that is placed on differences on individual dimensions; parameter r controls the progressive weight that is placed on larger differences between objects. If r and p are equal to 2, then this distance is equal to the Euclidean distance.

4.6.2.5 Percent disagreement

This measure is particularly useful if the data for the dimensions included in the analysis are categorical in nature. This distance is computed as:

$$\text{Distance}(x,y) = (\text{Number of } x_i \neq y_i) / i$$

4.6.3 Amalgamation or Linkage Rules

At the first step, when each object represents its own cluster, the distances between those objects are defined by the chosen distance measure. However, once several objects have been linked together, a linkage or amalgamation rule to determine when two clusters are sufficiently similar to be linked together is to be determined. There are various

possibilities: for example, two clusters can be linked together when *any* two objects in the two clusters are closer together than the respective linkage distance. Put another way, the "nearest neighbors" across clusters principle can be used to determine the distances between clusters; this method is called *single linkage*. This rule produces "stringy" types of clusters, that is, clusters "chained together" by only single objects that happen to be close together. Alternatively, the neighbors across clusters that are furthest away from each other can also be used; this method is called *complete linkage*. There are numerous other linkage rules such as these that have been proposed.

4.6.3.1 Single linkage (nearest neighbor)

As described above, in this method, the distance between two clusters is determined, by the distance of the two closest objects (nearest neighbors) in the different clusters. This rule will, in a sense, *string* objects together to form clusters, and the resulting clusters tend to represent long "chains".

4.6.3.2 Complete linkage (furthest neighbor)

In this method, the distances between clusters are determined, by the greatest distance between any two objects in the different clusters (i.e., by the "furthest neighbors"). This method usually performs quite well in cases when the objects actually form naturally distinct "clumps." If the clusters tend to be somehow elongated or of a "chain" type nature, then this method is inappropriate.

4.6.3.3 Unweighted pair-group average

In this method, the distance between two clusters is calculated as the average distance between all pairs of objects in the two different clusters. This method is also very efficient when the objects form natural distinct "clumps," however, it performs equally well with elongated, "chain" type clusters. The abbreviation UPGMA is widely used to refer to this method as *unweighted pair-group method using arithmetic averages*.

4.6.3.4 Weighted pair-group average

This method is identical to the *unweighted pair-group average* method, except that in the computations, the size of the respective clusters (i.e., the number of objects contained in them) is used as a weight. Thus, this method (rather than the previous method) should be used when the cluster sizes are suspected to be greatly uneven. The abbreviation *WPGMA* is widely used to refer to this method as *weighted pair-group method using arithmetic averages*.

4.6.3.5 Unweighted pair-group centroid

The *centroid* of a cluster is the average point in the multidimensional space defined by the dimensions. In a sense, it is the *center of gravity* for the respective cluster. In this method, the distance between two clusters is determined as the difference between centroids. The abbreviation *UPGMC* is widely used to refer to this method as *unweighted pair-group method using the centroid average*.

4.6.3.6 Weighted pair-group centroid (median)

This method is identical to the previous one, except that weighting is introduced into the computations to take into consideration differences in cluster sizes (i.e., the number of objects contained in them). Thus, when there are (or one suspects there to be) considerable differences in cluster sizes, this method is preferable to the previous one. The abbreviation *WPGMC* is widely used to refer to this method as *weighted pair-group method using the centroid average*.

4.6.3.7 Ward's method

This method is distinct from all other methods because it uses an analysis of variance approach to evaluate the distances between clusters. In short, this method attempts to minimize the Sum of Squares (SS) of any two (hypothetical) clusters that can be formed

at each step. In general, this method is regarded as very efficient, however, it tends to create clusters of small size.

4.6.4 Using Distances to Group Objects

After the distances between objects have been found, the next step in the cluster analysis procedure is to divide the objects into groups based on the distances. Again, any number of options are available to do this.

If the number of groups is known beforehand, a "flat" method might be preferable. Using this method, the objects are assigned to a given group at the first step based on some initial criterion. The means for each group are calculated. The next step reshuffles the objects into groups, assigning objects to groups based on the object's similarity to the current mean of that group. The means of the groups are recalculated at the end of this step. This process continues recursively until no objects change groups. This idea is the basis for "k-means cluster analysis" available on SPSS/WIN and other statistical packages. This method works well if the number of groups match the data and the initial solution is reasonably close to the final solution.

4.6.5 Hierarchical clustering

Hierarchical clustering methods do not require preset knowledge of the number of groups. Two general methods of hierarchical clustering methods are available: divisive and agglomerative.

The divisive techniques start by assuming a single group, partitioning that group into subgroups, partitioning these subgroups further into subgroups and so on until each object forms its own subgroup. The agglomerative techniques start with each object describing a subgroup, and then combine like subgroups into more inclusive subgroups until only one group remains.

4.6.6 Non Hierarchical clustering

In non-hierarchical clustering, the events are allocated to N clusters in such a way that, within the cluster, sum of squares of deviations from their respective means is minimized. The primary inputs are observations in the form of a matrix, the number of clusters, and the number of initial cluster centers. Selection of initial seed points or cluster centers is an important step in this method.

4.7 PRESENT STUDY

In order to ascertain the defect in composite specimens using wavelet analysis, the following procedure has been adopted in the present case, where through scanning has been used in both the modes of generation of ultrasonics by Lasers and conventional piezo-electric means:

- (1) For each A-scan signal $r_{x,y}(t)$ for $x = 1, \dots, N_x$ and $y = 1, \dots, N_y$, where the indices x and y indicate the spatial coordinates of the A-scan signal, N_x and N_y are the number of rows and lines of the C-scan respectively
 - (a) Generate discrete signal $r(n)$ for the signal $r(t)$.
 - (b) Calculate the wavelet representation of $r(n)$ and produce in vectorial form W_r .
 - (c) Calculate \hat{d}_j for $H \leq j \leq L$.
 - (d) Determine the wavelet coefficient mean, \hat{m}_j , according to,

$$\hat{m}_j = \frac{1}{(N \setminus 2^j - w_j + 1)} \sum_{k=w_j}^{N \setminus 2^j} |\hat{d}_j(k)|$$

Where w_j defines the size of the window applied on the wavelet level at the scale 2^j .

- (e) Calculate the characterization parameter $C_{x,y}$ of the signal $r_{x,y}(t)$,

$$C_{x,y} = \left[\sum_{j=H}^L \hat{m}_j \right]^{-1}$$

This summation of the main wavelet coefficients retained at different frequency level ($H \leq j \leq L$) according to value m_j above allows us to take into account a possible shifting of frequency of the signal peak.

- (2) Produce a matrix C ($\dim(C) = N_x \times N_y$) made of all $c_{x,y}$; this matrix contains information on the presence of a bottom reflection.
- (3) Plot the image of the characterisation parameter (c) using Image processing toolbox available in Matlab.

To compare the results based on wavelets, with ones based on use of only clustering techniques, the hierarchical clustering method with agglomerative procedure has been adopted. Ward's criterion (based on within group variance) for similarity determination has been used. Here, the clustering procedure starts with each data unit as a separate cluster or group and at each successive stage, two groups are merged which results in minimum increase in the total within group error sum of squares. The within group error sum of squares, E_k , about their mean vector in any k^{th} cluster can be expressed as

$$E_k = \sum_{i=1}^n \sum_{j=1}^{m_k} (x_{ijk} - \bar{x}_{ik})^2 = \sum_{i=1}^n \sum_{j=1}^{m_k} x_{ijk}^2 - m_k \sum_{i=1}^n \bar{x}_{ik}^2$$

Where x_{ijk} is the data belonging to i^{th} of n variables for the j^{th} of m_k data units in the k^{th} of h clusters. The mean on the I^{th} variable for m_k data units in the k^{th} cluster is expressed as

$$\bar{x}_{ik} = \sum_{j=1}^{m_k} x_{ijk} / m_k$$

The total within group sum of squares for the collection of clusters E is expressed as

$$E = \sum_{k=1}^h E_k$$

To begin with, there are NE data units, each a cluster onto itself and as such $E_k = 0$ for all the clusters. At any stage if clusters p and q are chosen to be merged and the resulting cluster is denoted by t , then the increase in E is

$$\Delta E_{pq} = E_t - E_p - E_q$$

$$\begin{aligned}
&= \left[\sum_{i=1}^n \sum_{j=1}^{\bar{m}_t} x_{ijt}^2 - m_t \sum_{i=1}^n \bar{x}_{it}^2 \right] - \left[\sum_{i=1}^n \sum_{j=1}^{\bar{m}_p} x_{ijp}^2 - m_p \sum_{i=1}^n \bar{x}_{ip}^2 \right] - \\
&\left[\sum_{i=1}^n \sum_{j=1}^{\bar{m}_q} x_{ijq}^2 - m_q \sum_{i=1}^n \bar{x}_{iq}^2 \right] \\
&= m_p \sum_{i=1}^n \bar{x}_{ip}^2 + m_q \sum_{i=1}^n \bar{x}_{iq}^2 - m_t \sum_{i=1}^n \bar{x}_{it}^2
\end{aligned}$$

since all the terms involving x_{ijk}^2 cancel. The mean on the I^{th} variable for the new cluster is found from the relation

$$m_t \bar{x}_{it} = m_p \bar{x}_{ip} + m_q \bar{x}_{iq}$$

squaring both sides of the equation gives

$$m_t^2 \bar{x}_{it}^2 = m_p^2 \bar{x}_{ip}^2 + m_q^2 \bar{x}_{iq}^2 + 2m_p m_q \bar{x}_{ip} \bar{x}_{iq}$$

The product of the means can be rewritten as

$$2 \bar{x}_{ip} \bar{x}_{iq} = \bar{x}_{ip}^2 + \bar{x}_{iq}^2 - (\bar{x}_{ip} - \bar{x}_{iq})^2$$

so that

$$m_t^2 \bar{x}_{it}^2 = m_p (m_p + m_q) \bar{x}_{ip}^2 + m_q (m_p + m_q) \bar{x}_{iq}^2 - m_p m_q (\bar{x}_{ip} - \bar{x}_{iq})^2$$

Noting that $m_t = m_p + m_q$ and substituting the value of \bar{x}_{it}^2 in equation, gives

$$\Delta E_{pq} = \frac{m_p m_q}{m_p + m_q} \sum_{i=1}^n (\bar{x}_{ip} - \bar{x}_{iq})^2$$

Thus it is seen that the minimum increase in the error sum of squares is proportional to the squared Euclidean distance between the centroids of the merged clusters. It is to be seen that the error sum of squares function E is non-decreasing and the method is not subject to reversals.

The code used by Datta [4] is based on the stored data approach where all of the original data is loaded in the central memory of the computer. If the similarities between any two

groups i and j is termed as S_{ij} then at the beginning, all possible S_{ij} s are computed and stored as elements of the similarity matrix. The most similar groups are identified by scanning the entries (S_{ij}) in the matrix. Only half the matrix is scanned, as it is symmetric. After each merger, the identification of the entities in the merged cluster is done and subsequently the S_{ij} entries are suitably updated to be used in the next pass. The procedure continues till the desired number of clusters are left out.

4.8 CLOSURE

In this Chapter, the basis of Cluster analysis, Signal Processing techniques like FT, STFT etc and later day techniques like Wavelet Transform (WT) have been presented, with special reference to their role in detection of defects in composite materials. The algorithm used for image generation based on cluster analysis has been discussed in detail. Some of the important mother wavelets and their properties have been discussed. Noise removal using multi-level DWT, which has been used in the present work, has also been explained. The procedure to obtain defect image generation using data compression technique inherent in wavelet analysis and algorithm to do the same have also been presented in this chapter.

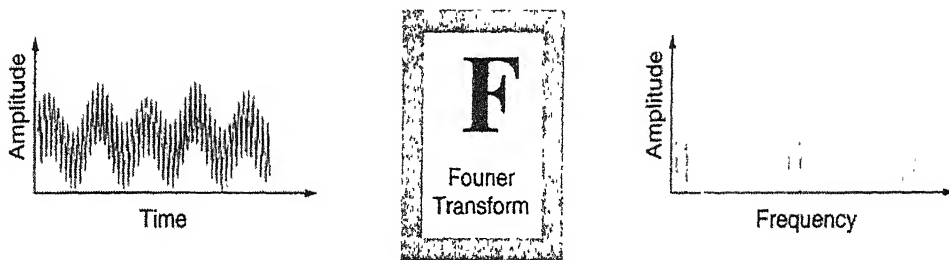
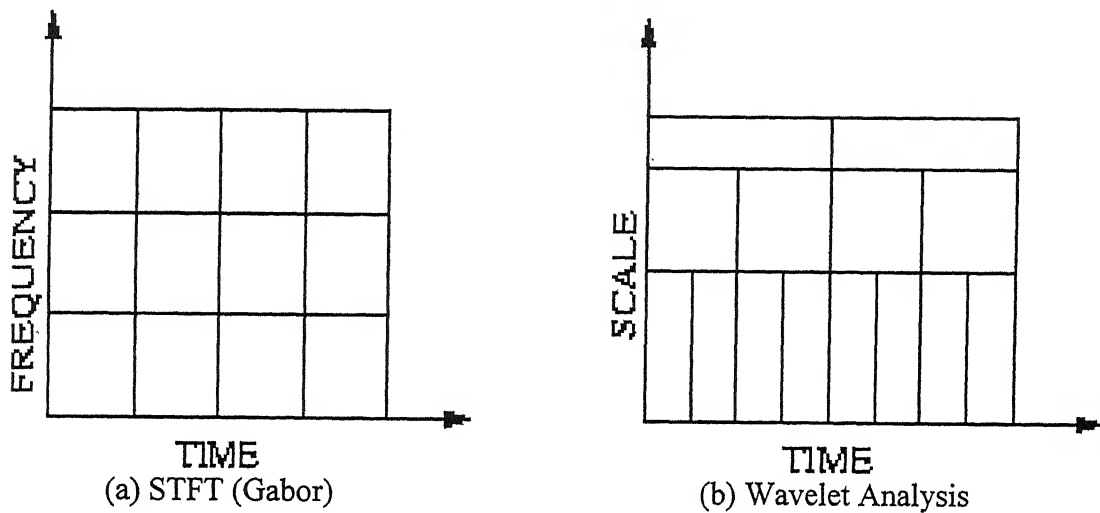


Fig. 4.1 Fourier Transform for transforming a time-domain signal to frequency-domain



Figs. 4.2(a-b) Short-Time Transform (Time-frequency domain), Wavelet Transform (Time-scale domain)

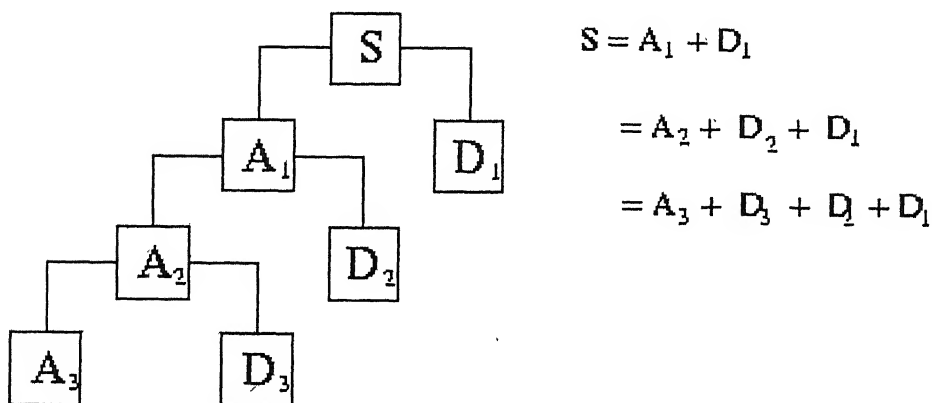


Fig. 4.3 Multiple-Level Wavelet decomposition tree with three-level decomposition

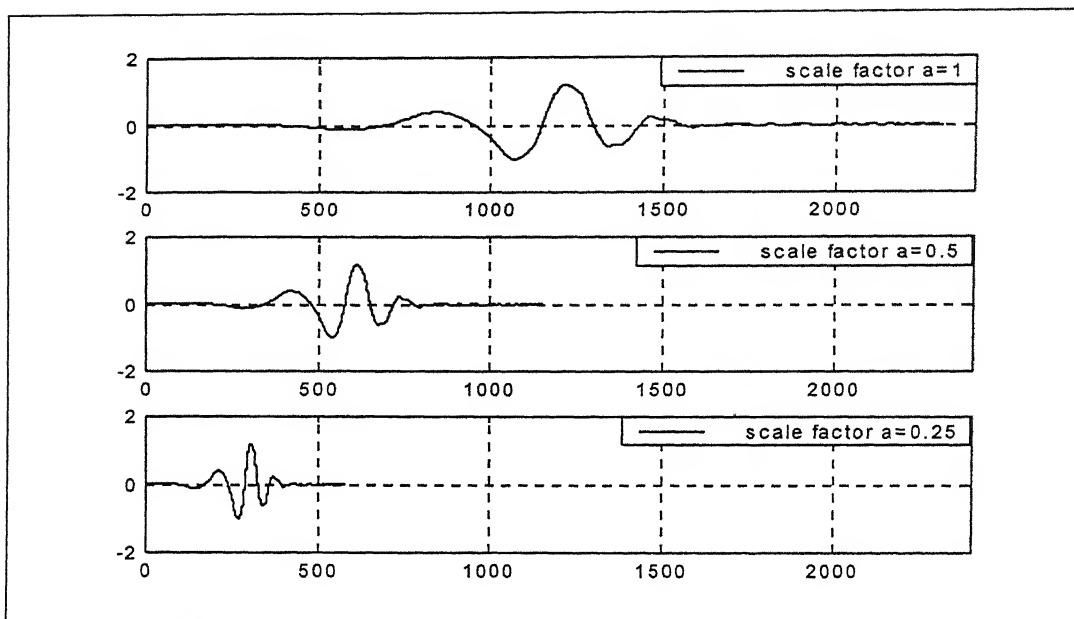


Fig. 4.4 Scaling (stretching or compression) of the wavelets with different scale factors

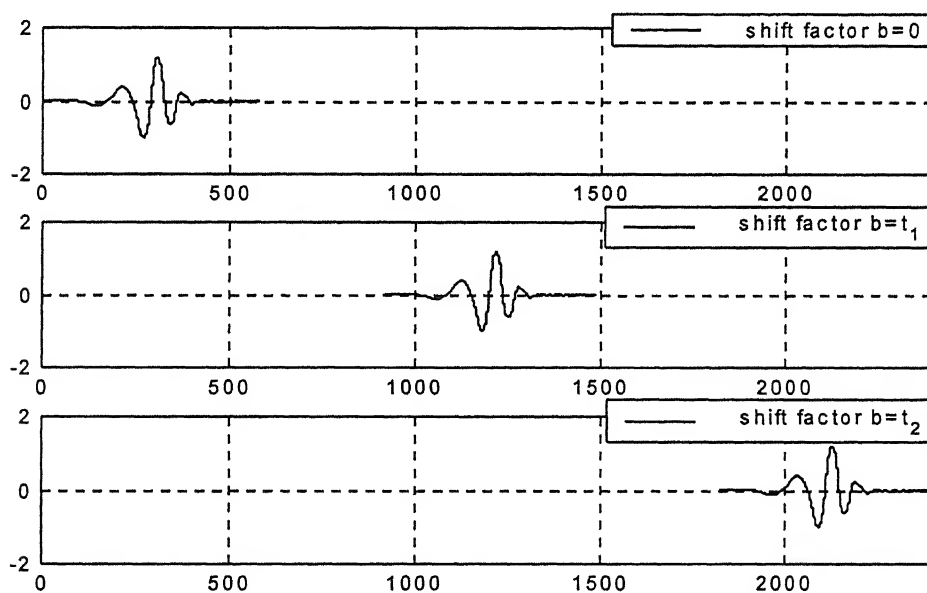
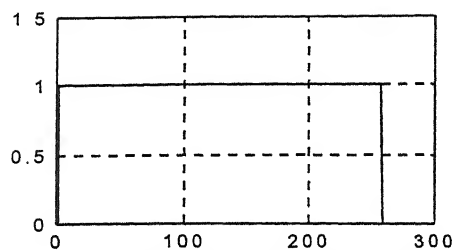
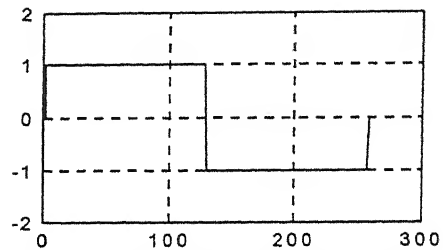


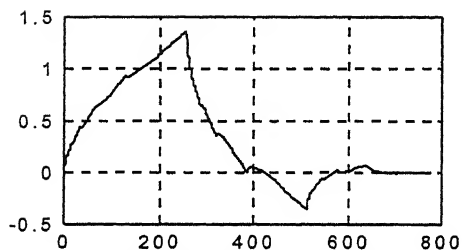
Fig. 4.5 Shifting (delaying or hastening) of the wavelets with different shift parameters



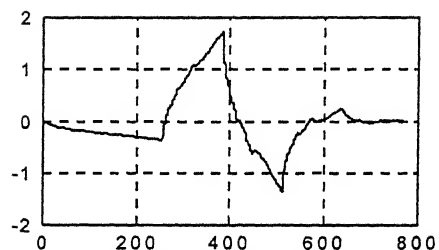
(a) db1/Haar Scaling function



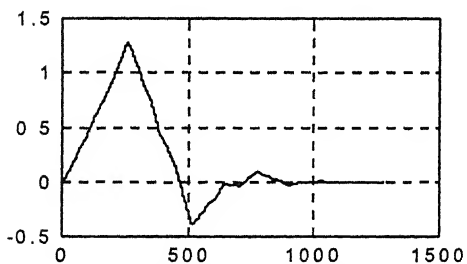
(b) db1/Haar Wavelet function



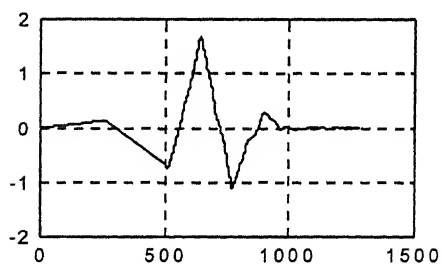
(c) db2 Scaling function



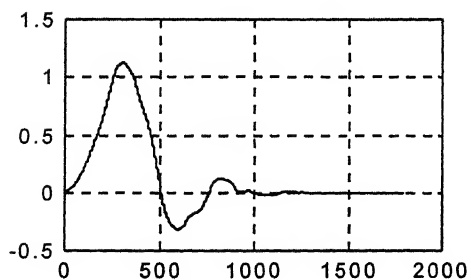
(d) db2 Wavelet function



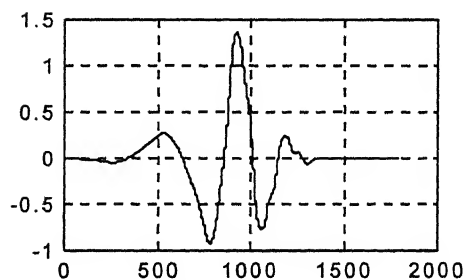
(e) db3 Scaling function



(f) db3 Wavelet function

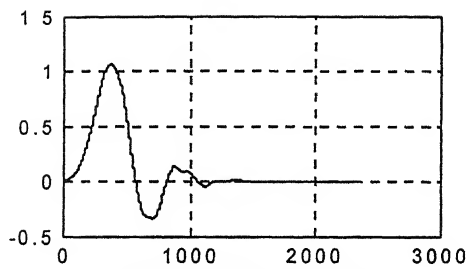


(g) db4 Scaling function

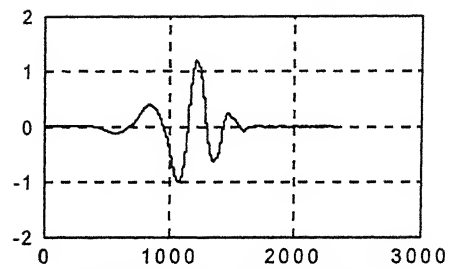


(h) db4 Wavelet function

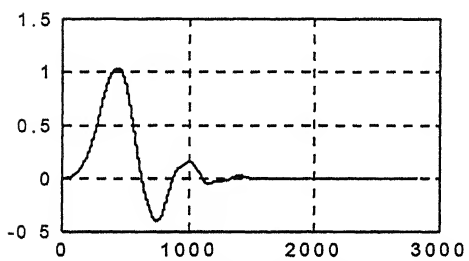
Figs. 4.6(a-h) Different wavelets (Daubechies) scaling and wavelet functions



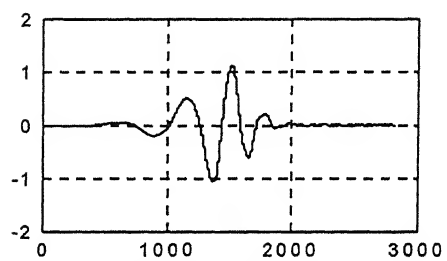
(i) db5 Scaling function



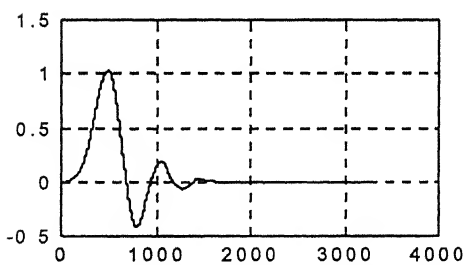
(j) db5 Wavelet function



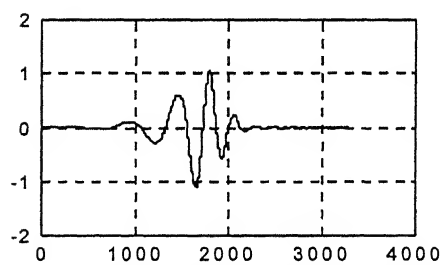
(k) db6 Scaling function



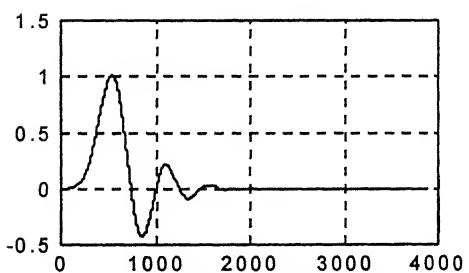
(l) db6 Wavelet function



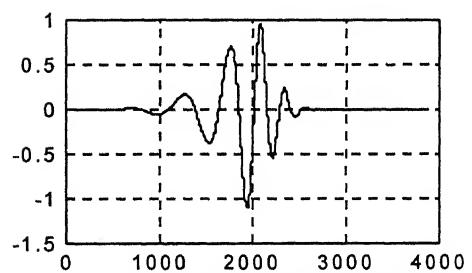
(m) db7 Scaling function



(n) db7 Wavelet function



(o) db8 Scaling function



(p) db8 Wavelet function

Figs. 4.6(i-p) Different wavelets (Daubechies) scaling and wavelet functions

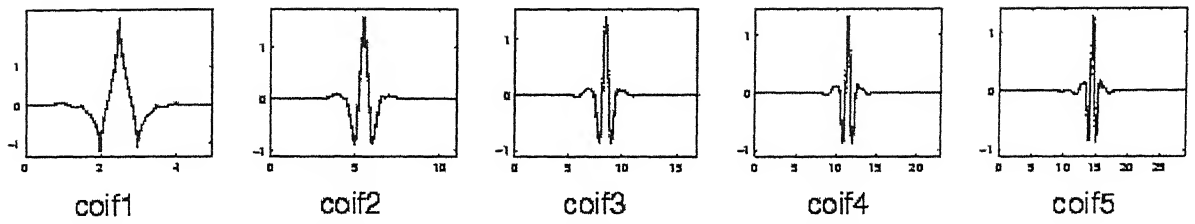


Fig 4.6(q) Coiflets in order from Coif1 to Coif5

RESULTS AND DISCUSSION

In the present study, an experimental technique has been developed using an Nd: YAG pulsed laser for generation of ultrasonic waves and a He-Ne continuous laser based heterodyne optical interferometric probe for detection. Tests were conducted on various composite specimens. Following is the results and discussions of these investigations.

5.1 Experiment Details

Composite specimens were fabricated with artificial inclusions like Teflon inserts and Resin rich zones. Diagrammatic representation of these samples is shown as Fig 5.1 (a) and (b). Laser Based Ultrasonics was used for inspection of these specimens. Averaging techniques were used to obtain sufficient signal to noise ratio. Here 32 averages were used. The same specimens were also inspected using water submerged conventional ultrasonics facility available, in the laboratory. The amplitudes of different harmonics are obtained after performing FFT on the received signals and these are stored in separate files, which are used for further analysis. Signals recorded (using LBU) at non-defective region and defective regions of specimens are shown in Fig 5.2 (a) to (j). The detected wave includes a pulsive noise signal induced by pulsed laser irradiation and random noise, which is inversely proportional to the intensity of the beat signal. As can be seen clearly from these figures, there is a difference between the waveforms obtained from the defective and non- defective regions. This is true for both cases of specimens with delaminations and resin rich zones. Please note that the waveforms and not the amplitudes are important criteria to identify the defects.

5.2 Cluster Analysis

After FFT on all signals, amplitudes of first fifty harmonics (frequency from 0.24 to 12.0 MHz in steps of 0.24 MHz) were recorded. Clustering was carried out using data corresponding to different harmonics, using the algorithm developed by Datta [4]. The

number of clusters was set as 10. C-scan images were then drawn from these cluster groups by assigning representative grey level to each scanned location depending on the cluster to which it belongs. Some typical C-scan images generated from the cluster analysis output, for peak amplitude of the individual harmonics is shown in Fig 5.3(a) to 5.3(q). As shown in [4], the best images correspond to frequency components of 1.2, 1.44 and 1.68 MHz. for specimens with Teflon inserts and for the specimens with Resin rich region, the images have been plotted for frequencies components of 7.68 and 7.92 MHz.

The results for the specimens with central inserts, generated by utilising the LBU setup data, have been encouraging, but are still not close to those achieved by using the conventional setup. The results for the specimens with Resin rich zones, generated by both LBU and conventional Lasers are similar, but would require improvement for facilitating use. This can be achieved by combining the harmonics to achieve better results as suggested by Datta [4]. The images generated for the specimen with the Teflon insert, are found to have a central region of lighter intensity, this is so, as the insert acts as a delamination and the high acoustical mismatch causes a strong reflection, furthermore the layered media effect of the composite system including the Teflon and adhering interfaces, however, will cause a modification of the pulse shape. The resin rich region is the one, where the signal attenuates rapidly and here we have a central region, which though not clearly demarcated is on a darker scale than the external non-resin rich boundaries.

The results of cluster analysis using data from conventional ultrasonics are better than those from LBU as one of the difficulties with using an optical technique for the detection of ultrasonic signals is the implementation of an automated system suitable for scanning large areas. Generally, laser light incident on a rough surface will be scattered diffusely into a large solid angle with a large amplitude specular reflection superimposed along the angle of reflection. The relative distribution of the specularly and diffusively reflected wave fields will thus vary depending on the component geometry and the local surface roughness at the probe spot reflection as the probe laser beam is scanned across the component surface. This results in an unpredictable variation in the LBU system sensitivity that is directly dependent on the angular reflectivity properties of the material being inspected. Fluctuations in detected ultrasonic signals amplitude will thus be

recorded regardless of the presence or absence of any defect, leading to ambiguities in signal interpretation. Thus signal interpretation based on only waveform and not amplitude gives better results. However, it should be noted that scanning noise represents a problem for any detection modality if it is sufficient to cause dropouts in signal. This is exactly what happened during scanning in a large number of cases. The control signal emanating from the heterodyne probe was found below the measurement threshold and hence this necessitated preamplification of the signal, which increased noise levels. Signals recorded using preamplification had higher noise levels. This caused errors in the data used for image generation (Both the clustering and wavelet coefficient extraction methods can have large-scale errors in case of deviations of maximal and minimal readings). Signals recorded using preamplification factors in excess of 1 are shown in Fig 5.4(a) to (f). Furthermore, reduction of scanning noise was not possible due to inadequacies of setup as only a single axis adjustment was available. In addition to scanning noise, fluctuations in the generation laser energy can also contribute to the uncertainty in absolute ultrasonic amplitude. During inspection, the laser pulse energy impinged on a composite specimen needs to be monitored so that ultrasonic signal amplitudes can be adjusted to compensate for variations in the absorbed energy. This will successfully allow fluctuations in the ultrasonic signal amplitude, due to ultrasonic attenuation, to be separated from those due to variations in the incident generation laser energy. This variation was found to be extensive as can be seen in Fig 5.5(a) and (b).

5.3 Wavelet Analysis

A wavelet method is proposed to analyse the ultrasonic signals received during the inspection of reinforced composite materials. Wavelet coefficients are extracted, followed by an interpretation procedure based on compression of the available data. The characterization parameter $C_{x,y}$ of the signals are computed and imaging carried out using Image processing toolbox available in Matlab. The images of the specimens generated using data from laser based setup and conventional signals are shown in Fig 5.6(a) to (e). As can be seen the defects are not clearly identifiable as in the images using the same data but utilizing clustering. The results achieved are, however encouraging as they show

that, the interface between the defective and nondefective regions is identifiable. This proves that the feature extracted has been effective in discerning the defect zone. This result was consistent for both the types of specimens tested, i.e., Composite specimens with insert and those with resin rich zones.

Certain additional defects have been identified in non-insert/ resin rich regions. However these are found using cluster analysis also and may be due to defects induced during manufacture. This can be seen clearly in Fig 5.7(a) to 5.7(d).

5.4 Closure

The results achieved by both methods on the new LBU setup are compared with those achieved using a conventional water submerged ultrasonic setup having fully automated c- scan facility.

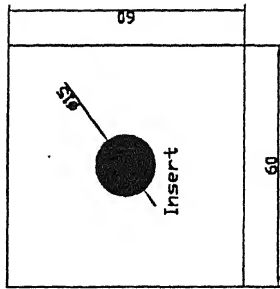


Fig 5.1(a)

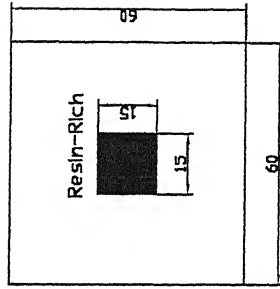


Fig 5.1(b)

Diagrammatic Representation of Specimens

Signals recorded on Insert Specimen

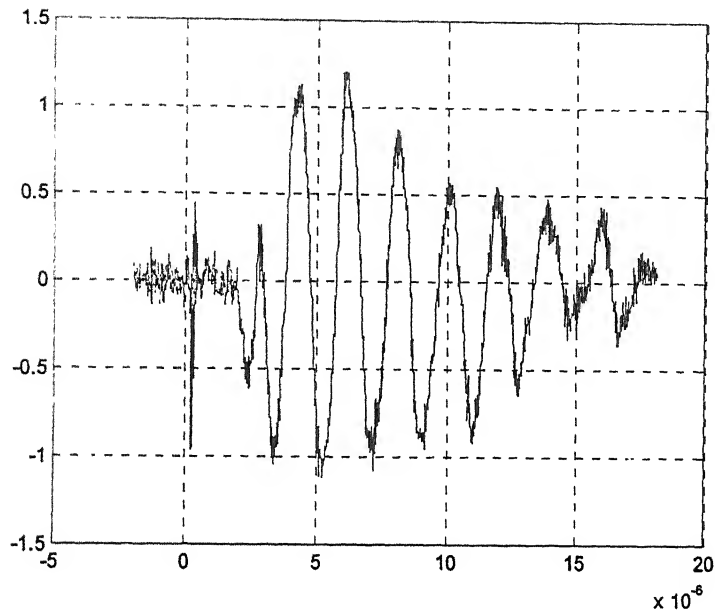


Fig 5.2 (a) Signal recorded in Non Insert zone

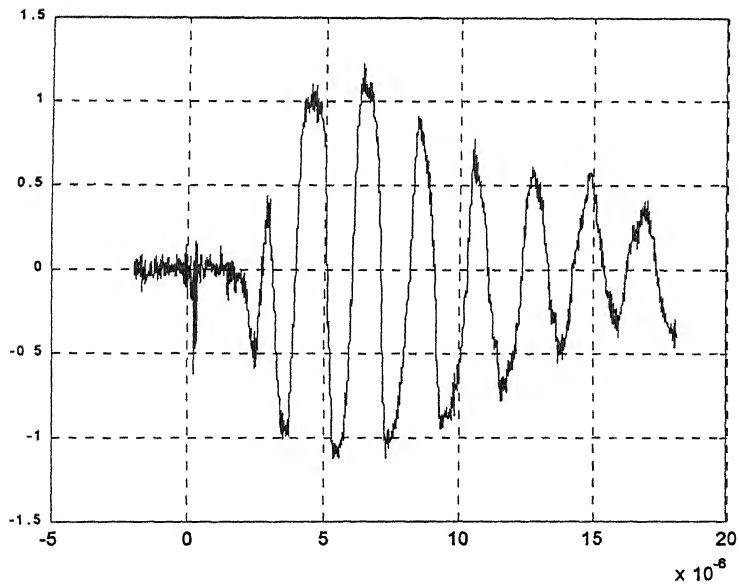


Fig 5.2(b) Signal recorded in Non Insert zone

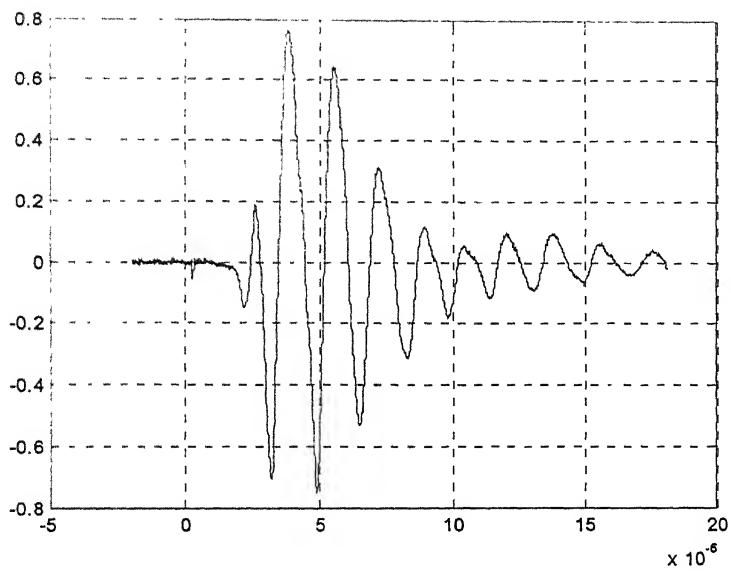


fig 5.2 (c) signal recorded in Non Insert zone

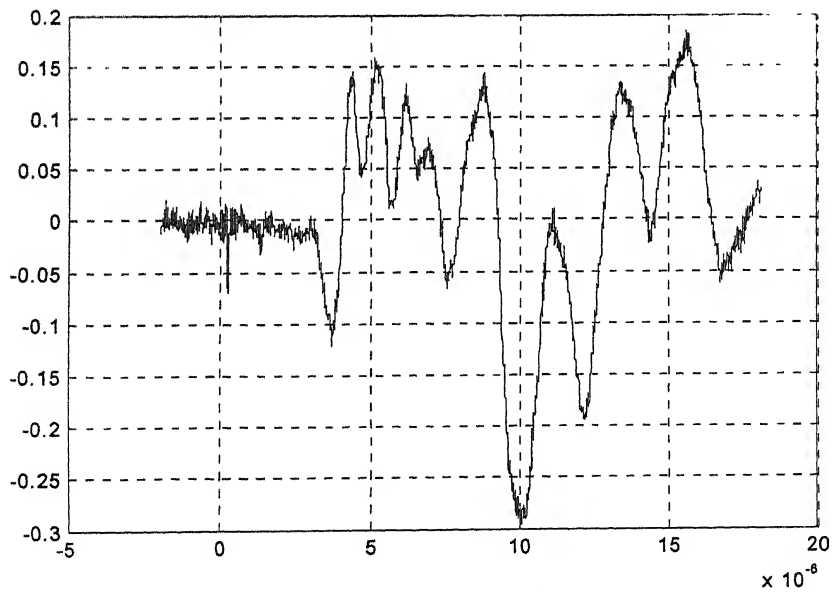


fig 5.2 (d) signal recorded in Insert zone

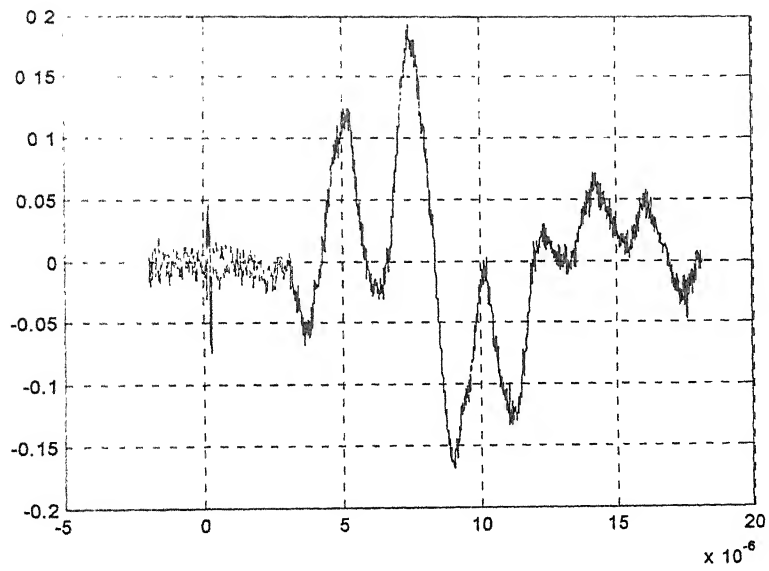


Fig 5.2 (e) Signal recorded in Insert zone

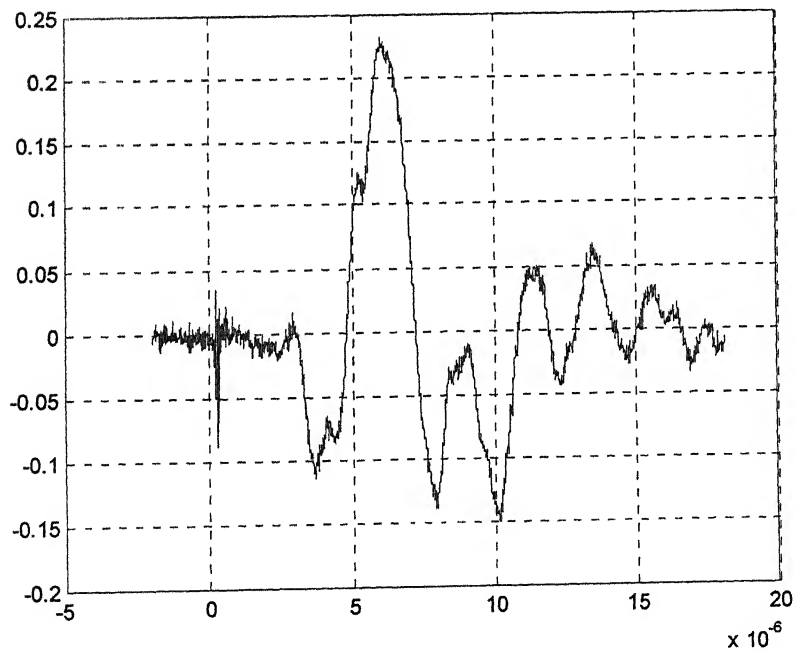


Fig 5.2 (f) Signal recorded in Insert zone

Signals recorded on Resin Rich Specimen

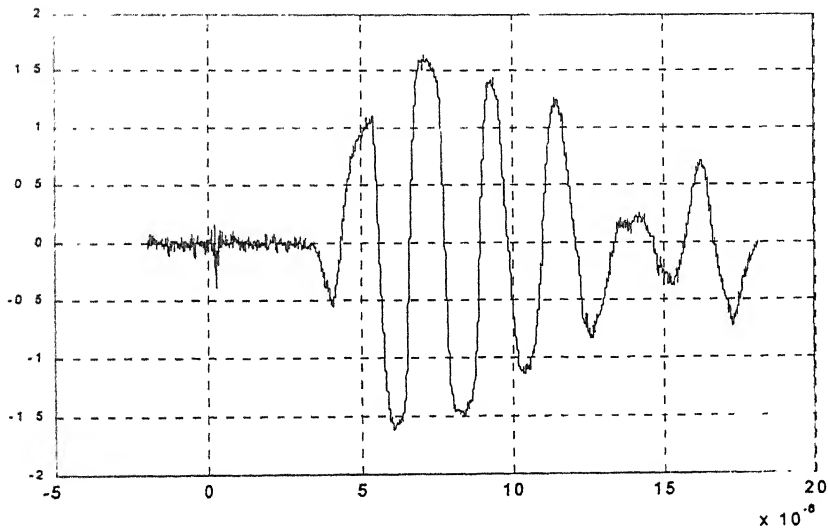


Fig 5.2 (g) Signal recorded in non resin rich region.

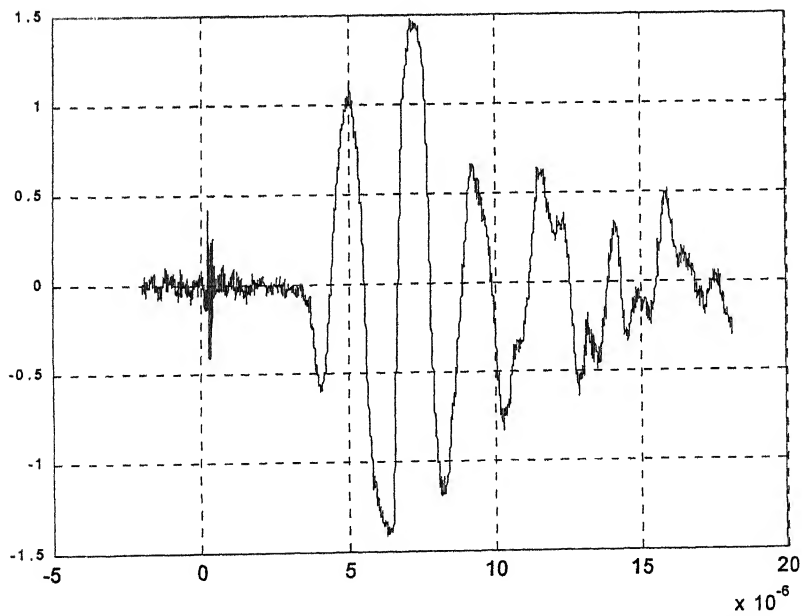


Fig 5.2 (h) Signal recorded in non resin rich region

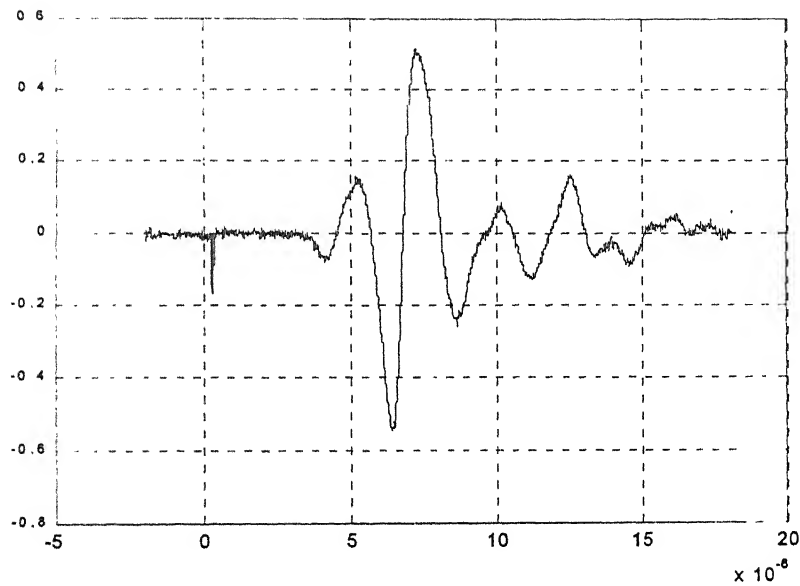


Fig 5.2 (i) Signal recorded in resin rich region.

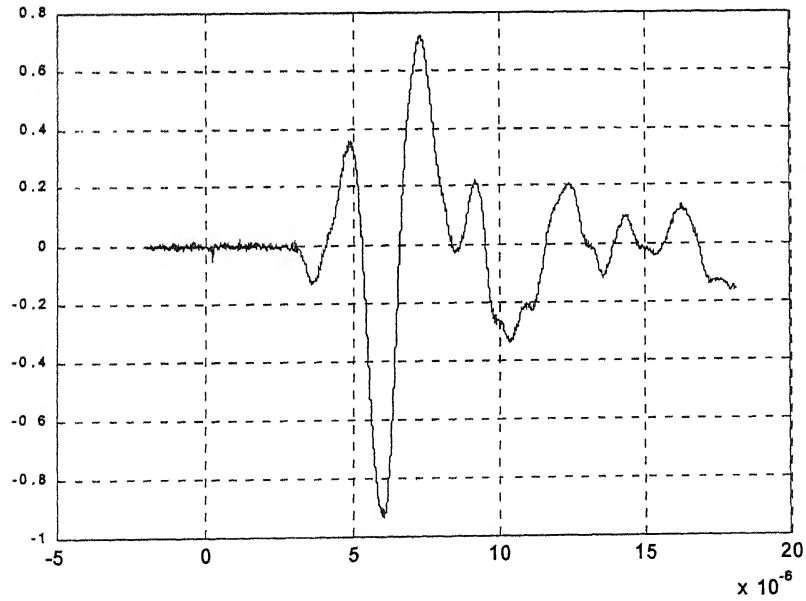


Fig 5.2 (j) Signal recorded in resin rich region.

IMAGES OF DEFECTS GENERATED USING CLUSTER ANALYSIS ON DATA GENERATED BY LASER BASED ULTRASONICS.

Results for Specimen with central Insert.

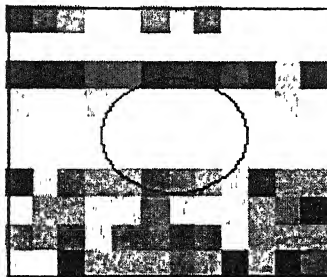


Fig. 5.3 (a) Image generated by using clustering freq 1.2 MHz

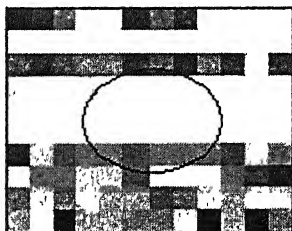


Fig. 5.3 (b) Image generated by using clustering freq 1.44 MHz

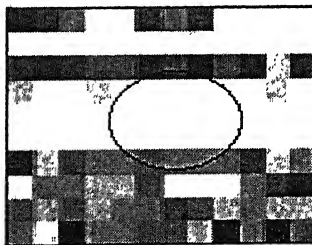


Fig. 5.3 (c) Image generated by using clustering freq 1.68 MHz

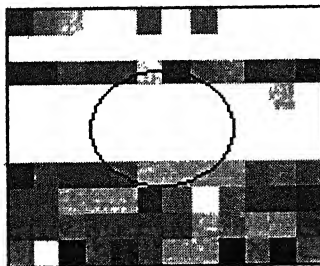


Fig. 5.3 (d) Image generated by using clustering freq 4.08 MHz

Results for Specimen with central Resin rich Zone.

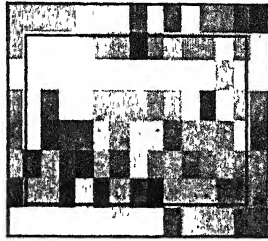


Fig. 5.3 (e) Image generated by using clustering

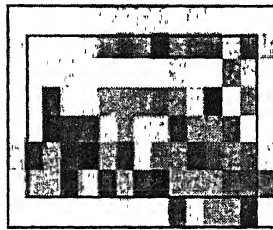


Fig. 5.3 (f) Image generated by using clustering

**IMAGES OF DEFECTS GENERATED USING CLUSTER ANALYSIS
ON DATA GENERATED BY CONVENTIONAL ULTRASONICS.**

Results for Specimen with central Insert.

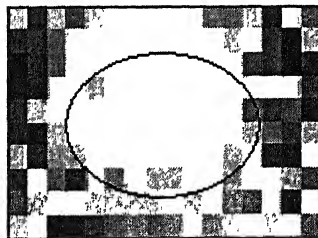


Fig. 5.3 (g) Image generated by using clustering

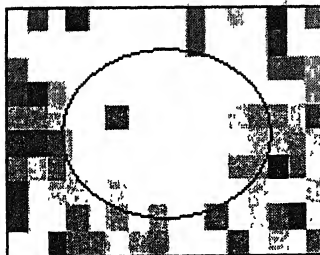


Fig. 5.3 (h) Image generated by using clustering freq 1.2MHz

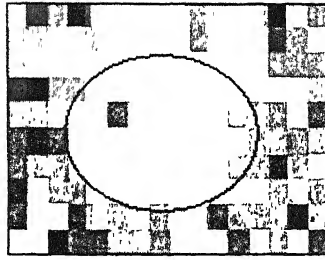


Fig. 5.3 (i) Image generated by using clustering freq 1.44MHz

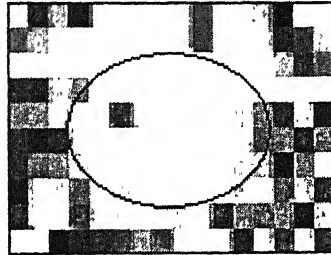


Fig. 5.3 (j) Image generated by using clustering freq 1.68MHz

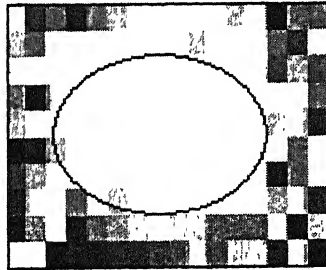


Fig. 5.3 (k) Image generated by using clustering freq 4.08MHz

Results for Specimen with central Resin rich Zone.

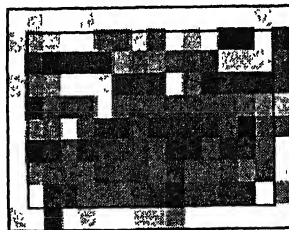


Fig. 5.3 (l) Image generated by using clustering

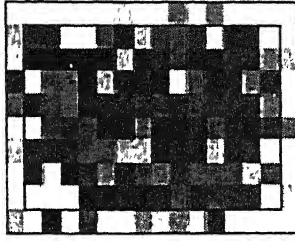


Fig. 5.3 (m) Image generated by using clustering freq 7.68 MHz

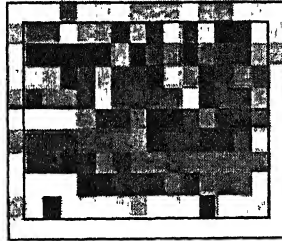


Fig. 5.3 (n) Image generated by using clustering freq 7.92 MHz

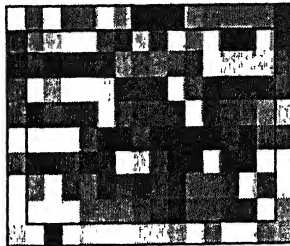


Fig. 5.3 (o) Image generated by using clustering

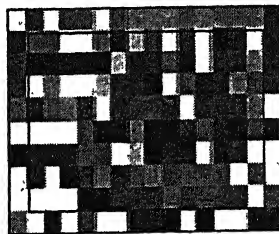


Fig. 5.3 (p) Image generated by using clustering freq 7.68 MHz

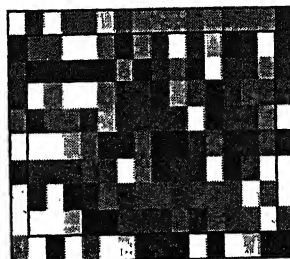


Fig. 5.3 (q) Image generated by using clustering freq 7.92 MHz

Signals recorded using preamplification facility in Electronic signal processing unit.

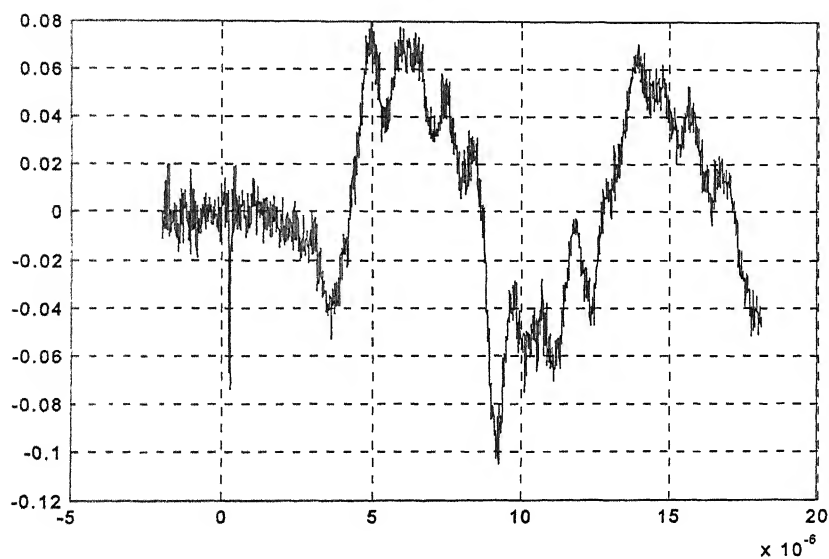


Fig 5.4 (a) Signal recorded in Insert zone using a preamplification factor 10.

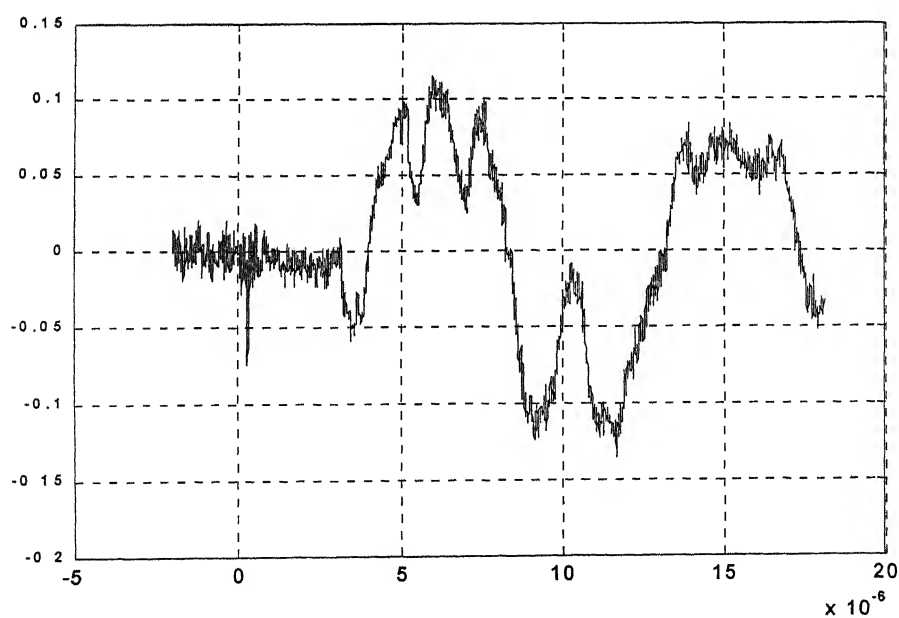


Fig 5.4 (b) Signal recorded in Insert zone using a preamplification factor 10.

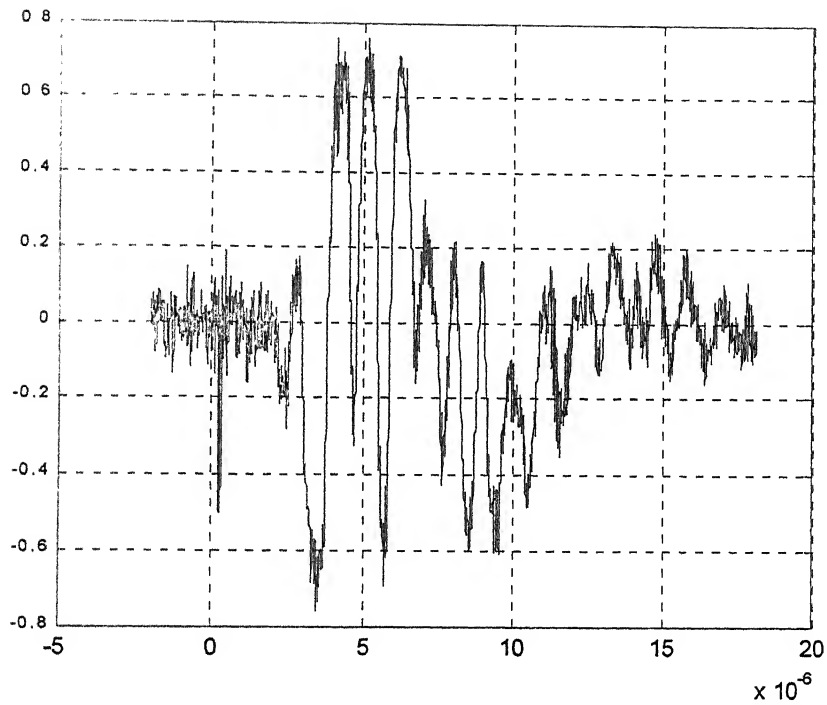


Fig 5.4 (c) Signal recorded in Non Insert zone using a preamplification factor 10.

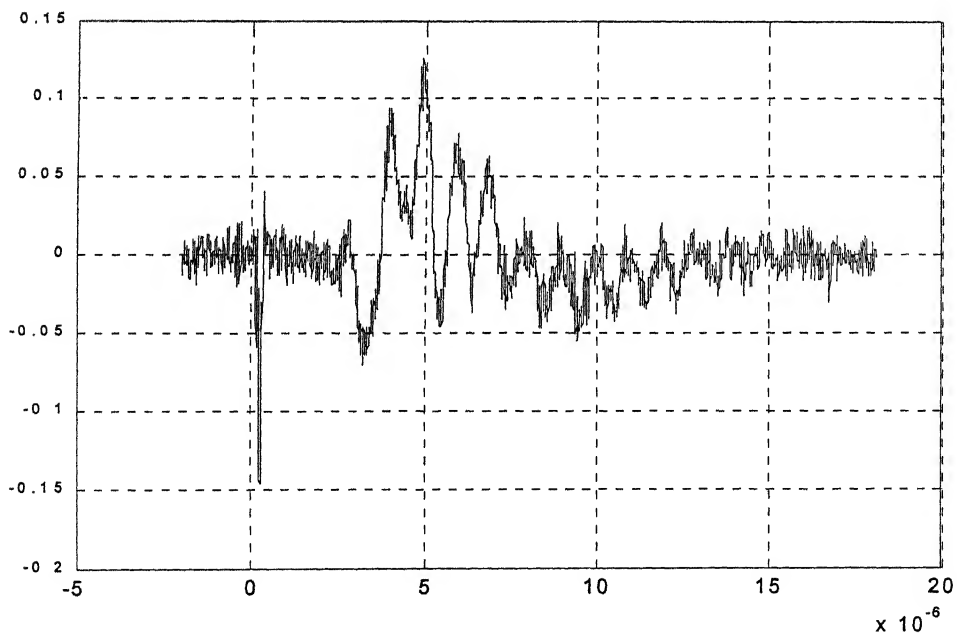


Fig 5.4 (d) Signal recorded in Non Insert zone using a preamplification factor 10.

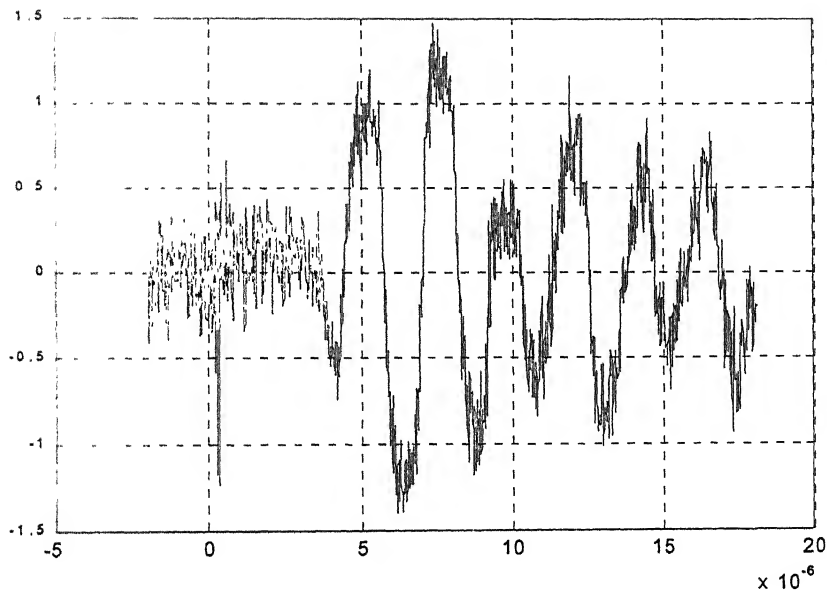


Fig 5.4 (e) Signal recorded in Non Resin rich zone using a preamplification factor 10.

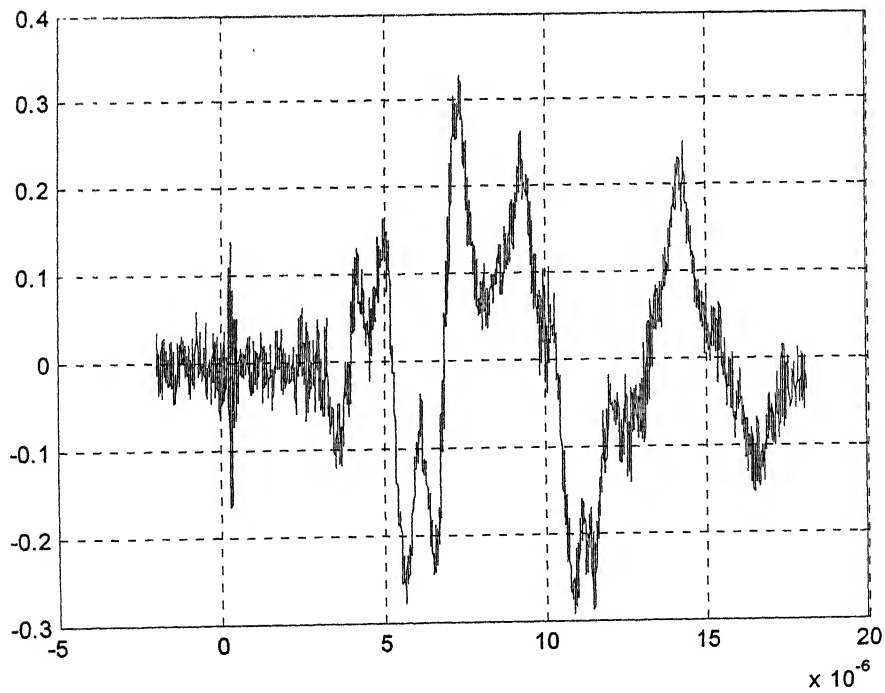


Fig 5.4 (f) Signal recorded in Resin rich zone using a preamplification factor 10.

VARIATION IN LASER GENERATION ENERGY.

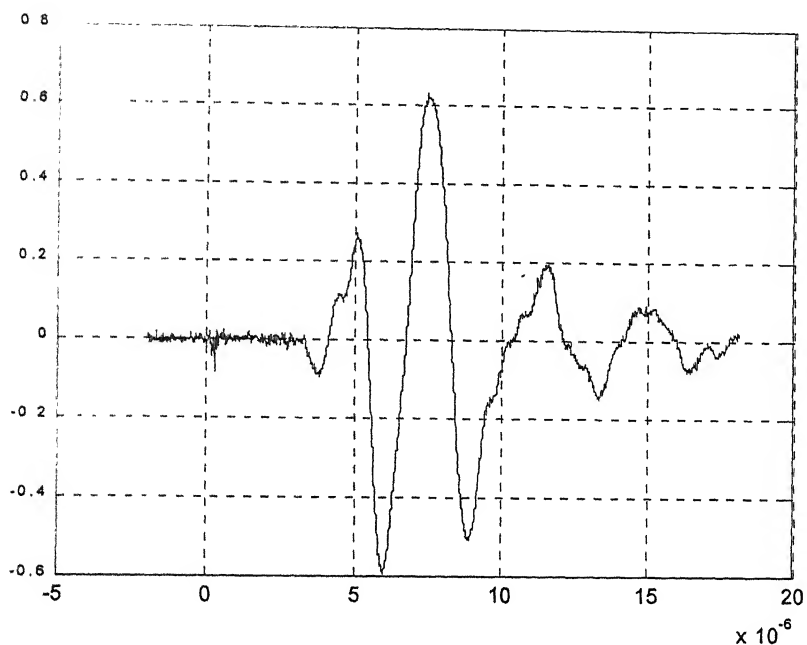


Fig 5.5(a) Signal taken outside resin rich region sudden reduction in noise and signal strength (laser power now stepped up to 18mJ from earlier 13.5mJ)

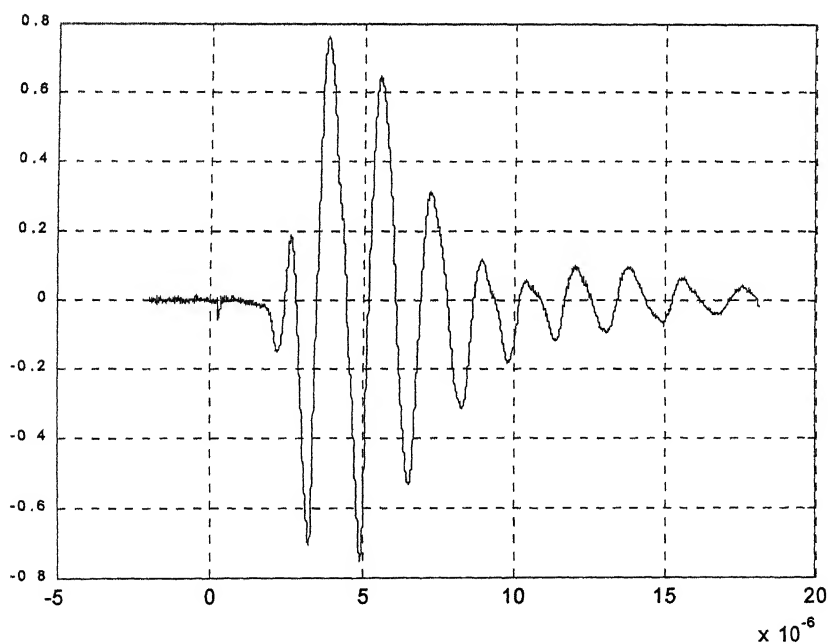


Fig 5.5(b) Signal outside Insert Region. sudden reduction in noise and signal strength (laser power now stepped up to 18mJ from earlier 13.5mJ)

**IMAGES OF DEFECTS GENERATED USING WAVELET
ANALYSIS ON DATA GENERATED BY CONVENTIONAL
ULTRASONICS.**

Results for Specimen with central Insert.



Fig 5.6(a) Insert Conventional by using Wavelets.

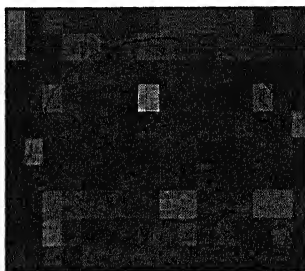


Fig 5.6(b) Insert Conventional using wavelets 02

Results for Specimen with central Resin rich Zone.

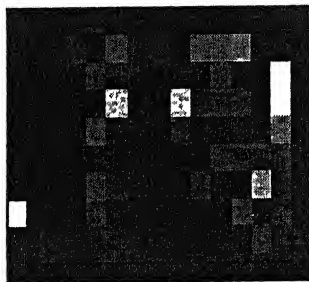


Fig 5.6(c) Resin Conventional by using Wavelets

**IMAGES OF DEFECTS GENERATED USING WAVELET ANALYSIS ON
DATA GENERATED BY LASER BASED ULTRASONICS.**

Results for Specimen with central Insert.

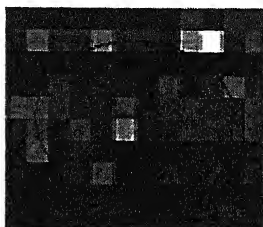


Fig 5.6(d) Insert Laser by using Wavelets.

Results for Specimen with central Resin rich Zone.

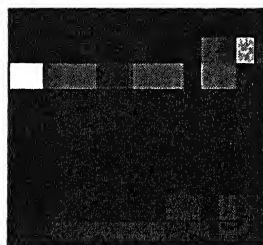


Fig 5.6(e) Resin Laser by using wavelets

**ADDITIONAL DEFECTS IDENTIFIED BY BOTH CLUSTERING AND
WAVELET ANALYSIS.**



Fig. 5.7(a) Image: Insert generated using wavelets

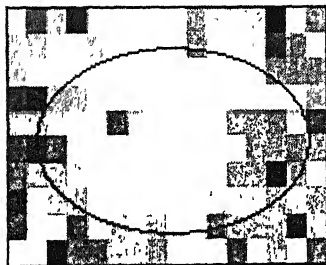


Fig. 5.7(b) Image: Insert generated by using clustering freq 1.44MHz

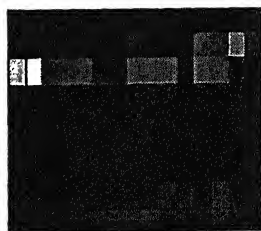


Fig. 5.7(c): Image: Resin generated by using wavelets

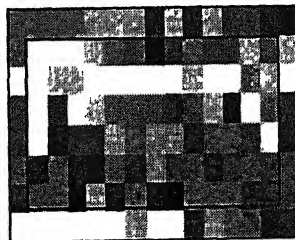


Fig. 5.7 (d) Image: Resin generated by using clustering

CONCLUSIONS AND SCOPE FOR FUTURE WORK

6.1 CONCLUSIONS

In the present work, an experimental technique has been developed using an Nd: YAG pulsed laser for generation of ultrasonic waves in specimens and a He-Ne continuous laser based heterodyne optical interferometric probe for detection of the same. Artificially implanted defective composite specimens have been scanned on this setup, and to facilitate comparison similar scanning has been carried out on conventional water submerged ultrasonics setup. Cluster analysis and wavelet analysis have been used to recreate images of the scan. Based on the results obtained, the following conclusions are drawn:

- (1) The Laser based Ultrasonics setup is capable of detecting abnormalities in composites, as is verifiable by the results of the cluster and wavelet feature extraction analysis.
- (2) The results achieved by wavelet analysis feature extraction technique are encouraging as it is able to identify the interface between the defective and nondefective regions.

6.2 SCOPE FOR FUTURE WORK

The problems encountered, namely reduction of scanning noise and fluctuations in energy levels of ultrasonic source laser can be reduced to minimize errors by

- (1) Exploring the possibility of applying paint, oil to irradiated surface as this may improve or alter ultrasonic characteristics as reported in literature for metallic specimens. This will also make it possible to use higher power settings without worrying about ablating the composite specimen.
- (2) A peelable retroreflective film has been identified for adhering onto surface interrogated by the heterodyne interferometer. This gives an approximately uniform response (<3 dB variation) over a scan on a relatively smooth surface. The retroreflective film uses a commercially available retroreflective paint (3M

scotchlite series), which comprises glass micro beads that have a hemispherical aluminum coating, and are contained in a liquid binder. This can be used to achieve better results.

- (3) An opaque specimen gives better results; the results would definitely be better for say graphite epoxy where the specimen is darker. Thicker specimens can be worked with to improve/ assess the efficacy of the technique.
- (4) The system can be made portable, and incorporating fiber optics for picking up the displacement of the surface from larger distances. Similarly the mechanical scanning requirements of the specimen can be overcome by resorting to use of an arrangement of optical mirrors and lenses for facilitating complete surface scan by motion of these optical components only.

References

- [1] Krautkramer Josef, Krautkramer Herbert. "Ultrasonic Testing of Materials", Springer-Verlag Berlin Heidelberg, New York, 1983.
- [2] Neslroth J.B., Rose J.L., Bashyam M. and Subramanian K., 1985, "Physically based ultrasonic feature mapping for anomaly classification in composite materials", Materials Evaluation, Vol. 43, pp. 541-546.
- [3] Rose J.L., 1984, "Elements of a feature based ultrasonic inspection system", Materials Evaluation, Vol. 40, pp. 210-226.
- [4] Datta, Debasis. "A Methodology in Ultrasonic NDE for Identification and Reconstruction of defects in Fiber Composites", Ph.D. Thesis, September 1995, Department of Mechanical Engineering, Indian Institute of Technology-Kanpur.
- [5] Scruby and Drain. "Laser Ultrasonics Techniques and Applications", Adam Hilger Bristol, Philadelphia and New York, 1990
- [6] Monchalin J.B., "Optical Detection of Ultrasound", IEEE Transactions on Ultrasonics, Ferroelectrics, and Frequency control, Vol UFFC-33, no. 5 September 1986, pp. 485-499
- [7] Huber R.D. and Green R.E., Jr., " Noncontact Acousto-Ultrasonics Using Laser Generation and Laser Interferometric Detection", Materials Evaluation May 1991, pp.613-618.
- [8] Christine Corbel, Franck Guillois, Daniel Royer, Mathias A. Fink, and Rene DE Mol, "Laser-Generated Elastic Waves in carbon-Epoxy Composite", IEEE Transactions on Ultrasonics, Ferroelectrics, and Frequency Control, Vol 40, No. 6, November1993, pp. 710-716
- [9] Jin Huang, Yasuaki Nagata, Sridhar Krishnaswamy and Jan D. Achenbach, "Laser Based Ultrasonics for Flaw Detection", 1994 Ultrasonics Symposium IEEE, pp. 1205-1209.
- [10] Castagnede B., Marc Deschamps, Eric Mottay and Andre Mourad, " Laser impact generation of ultrasound in composite materials", Acta Acustica 2 (April 1994), pp. 83-93.

- [11] Hideo Cho, Shingo Ogawa and Mikio Takemoto, "Non Contact laser ultrasonics for detecting subsurface lateral defects", NDT&E International, Vol 29, No.5, pp.301-306, 1996.
- [12] Hisashi Yamawaki, Tetsuya Saito, Hiroaki Fukuhara, Chitoshi Masuda, Yoshihisa Tanaka, "Non contact Ultrasonic Imaging of Subsurface Defects Using a Laser-Ultrasonic Technique", J. Appl. Phys. Vol. 35 (May 1996) pp. 3075-3079
- [13] Carlo Francesco Morabito. "Independent Component Analysis and Feature Extraction Techniques for NDT Data", Materials Evaluation, January 2000, pp. 85-92.
- [14] S.K. Rathore, N.N. Kishore, P. Munshi and W. Arnold, "Defect Location and Sizing Using Laser Based Ultrasonics (LBU)", Submitted for publication.
- [15] Legendre S., Goyette J., and Massicotte D. "Ultrasonic NDE of composite material structures using wavelet coefficients", NDT&E International, Vol. 34, No. 1, January 2001, pp. 31-37.

Appendix A

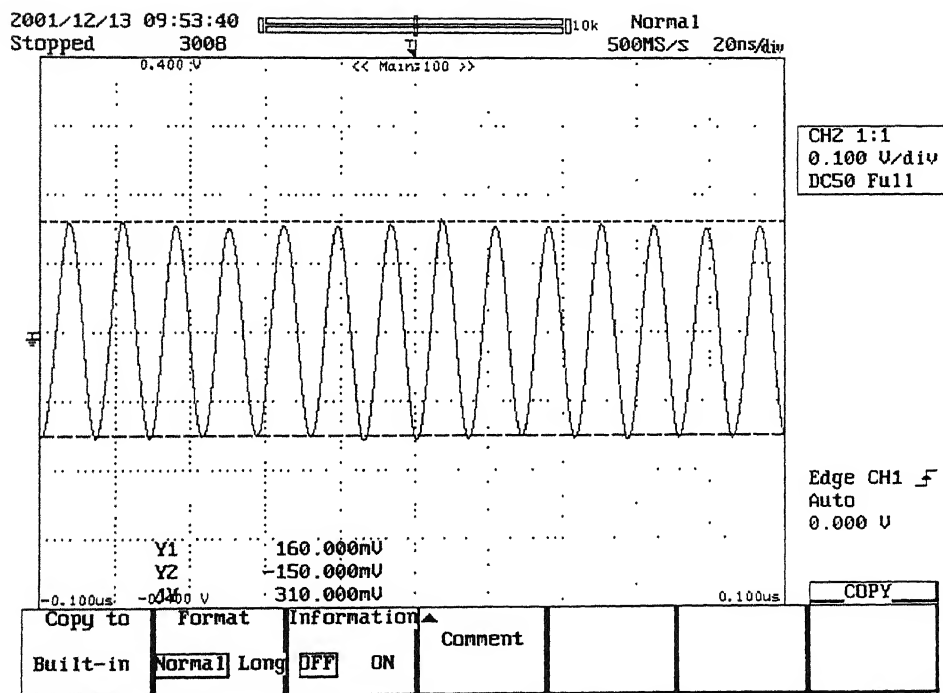
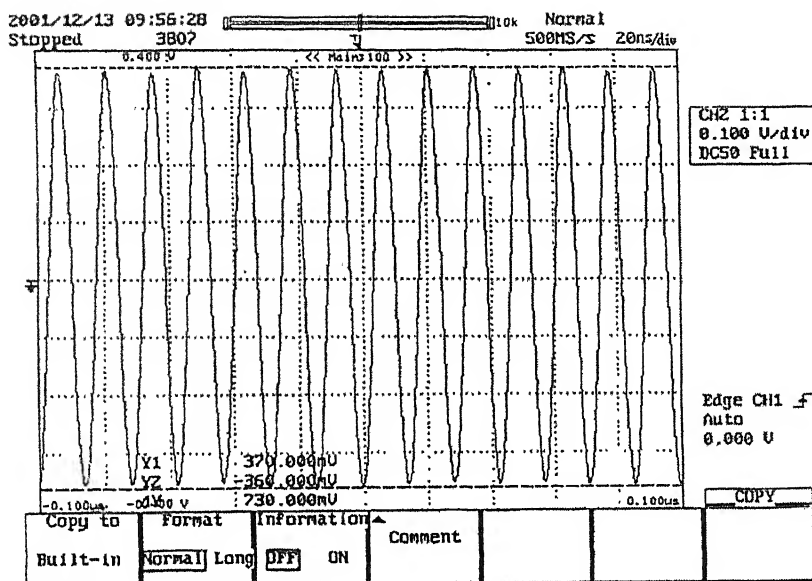
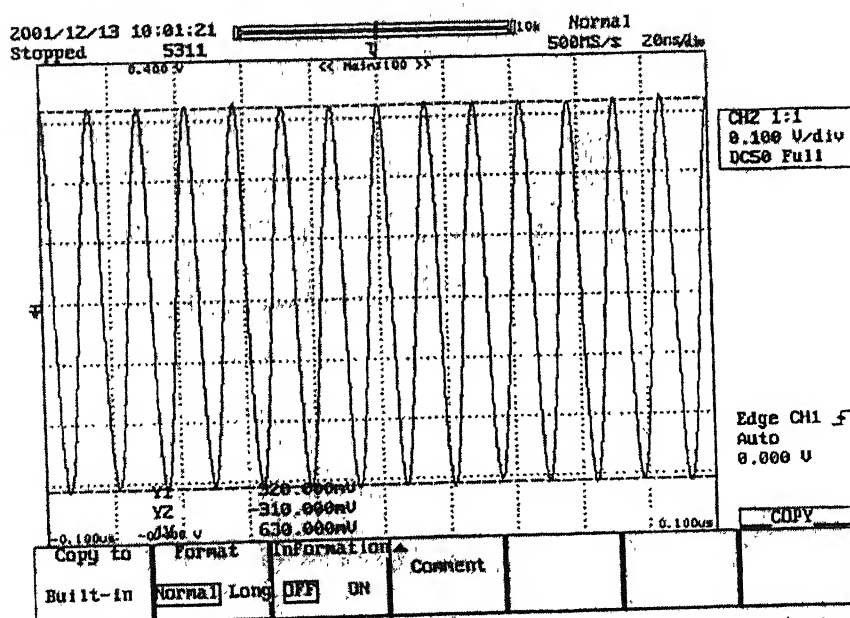


Photo Detector Output Measured Without Going Through The Signal Processor.

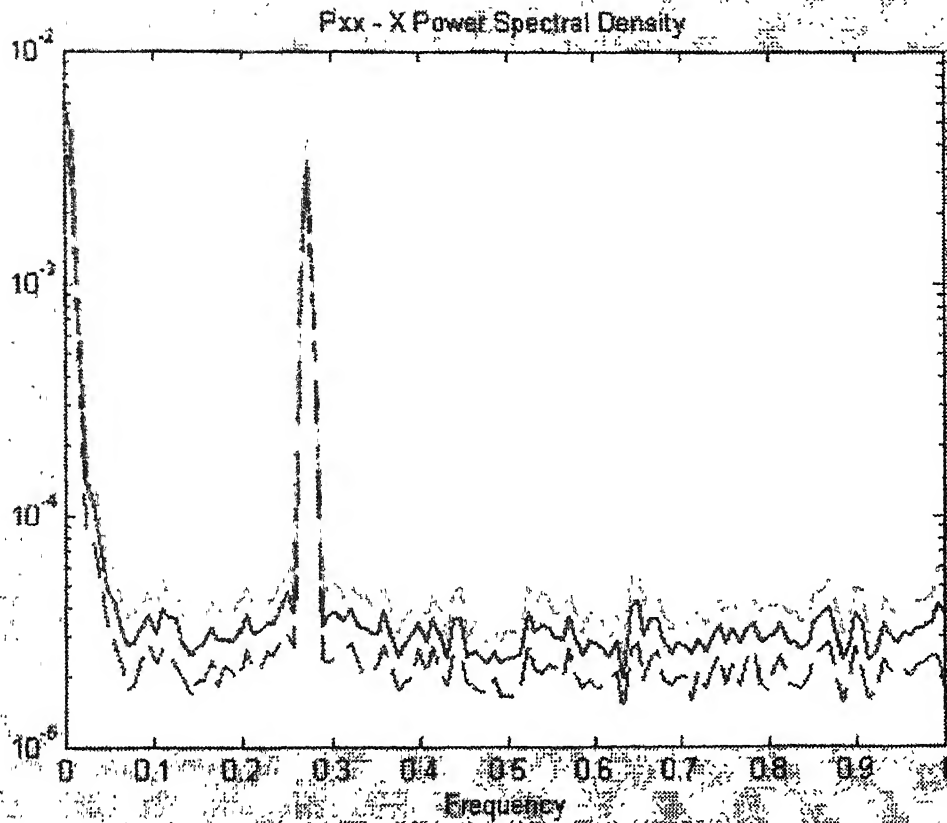
Appendix B



Output Taken Through The Signal Processor With The Automatic Gain Control Switched On.

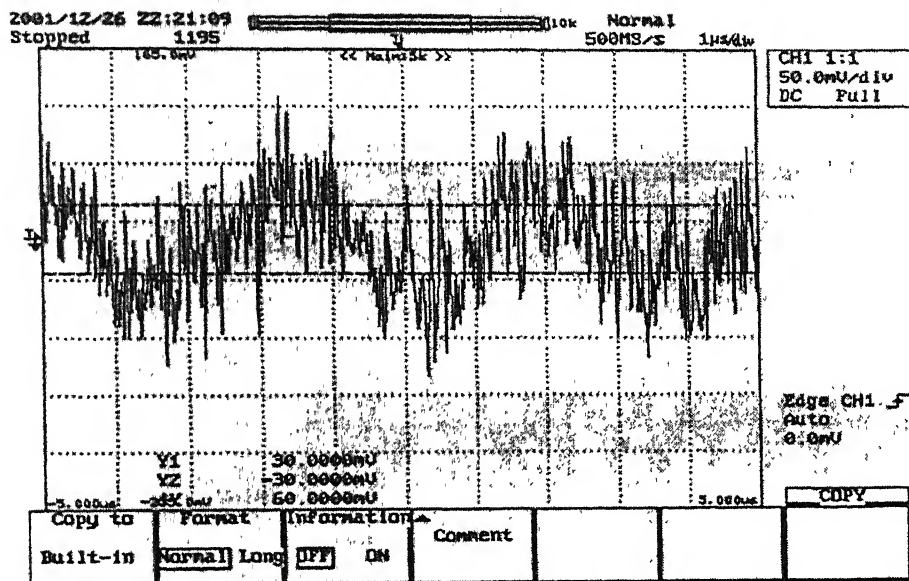


Output Taken Through The Signal Processor With The Automatic Gain Control Switched On After Making Adjustments Available In The Signal-Processing Unit In order To Set It To 630mv.

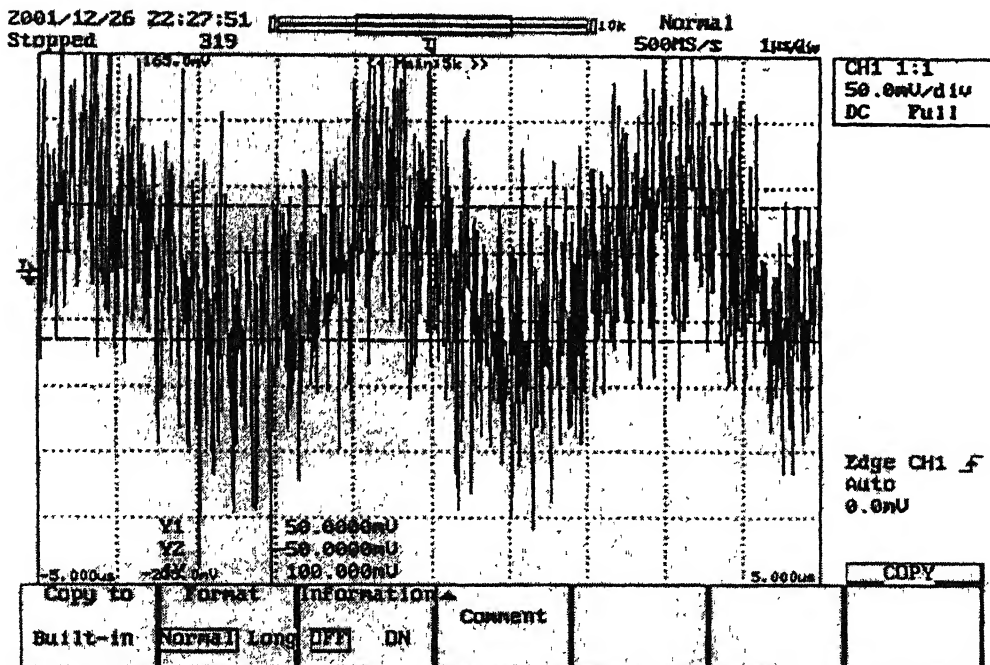


Power Spectrum Display In Matlab Used To Measure Sensitivity Of Heterodyne Interferometer. (The Measured Sensitivity Was 10 Mv/ A°.)

Appendix D



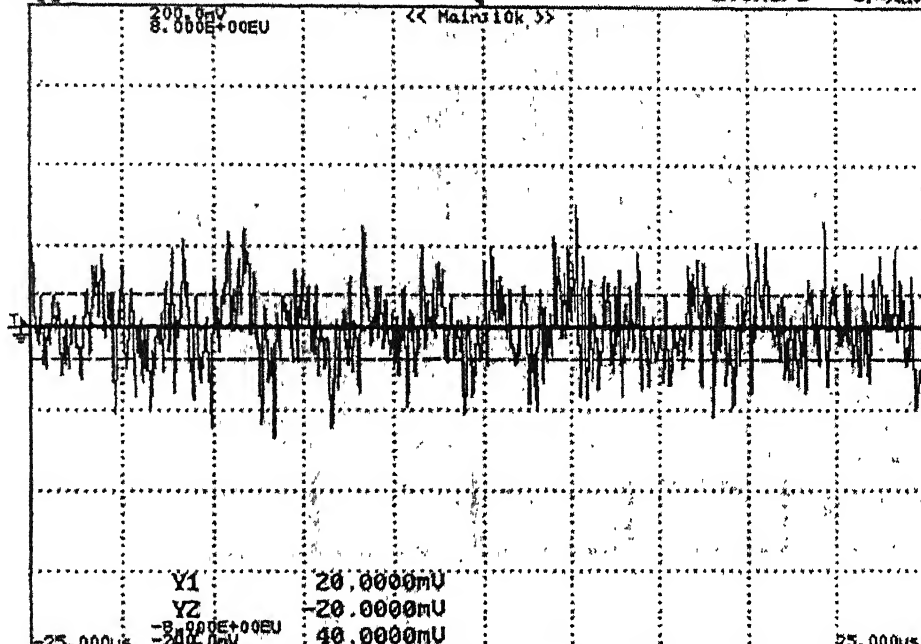
Detectivity Measurement (18MHz Bandwidth) Displacement $3A^\circ$



Detectivity Measurement (45MHz Bandwidth) Displacement $5A^\circ$

2001/12/25 23:14:00
Stopped 1464

10k Normal
200MS/s 5ns/div



CH1 1:1
50.0mV/div
DC Full

Math2
C3+C4

Edge CH1 ☒
Auto
0.0mV

Copy to		Format	Information ▲		COPY	
Built-in		Normal Long	OFF	ON	Comment	

Detectivity Measurement (4MHz Bandwidth) Displacement 2A°

Appendix E

%Matlab Program for extracting the characterisation parameter from coefficients at different levels after wavelet decomposition.

```
%loading the signal
load cr010201dnc;
s = cr010201dnc(1:512);
l_s = length(s);
%decomposing the signal
[C,L] = wavedec(s,5,'coif5');
%Extracting level 5 approximation coefficients from C
cA5 = appcoef(C,L,'coif5',5);
%Extracting levels 1,2,3,4,5 detail coefficients from C
[cD1,cD2,cD3,cD4,cD5] = detcoef(C,L,[1,2,3,4,5]);
%Reconstructing the level 5 approximation
A5 = wrcoef('a',C,L,'coif5',5);

%Reconstructing the level 1,2,3,4,5 details
D=zeros(5,512);
for j=1:5
D(j,:) =D(j,:)+ wrcoef('d',C,L,'coif5',j);
end
D1 = wrcoef('d',C,L,'coif5',1);
D2 = wrcoef('d',C,L,'coif5',2);
D3 = wrcoef('d',C,L,'coif5',3);
D4 = wrcoef('d',C,L,'coif5',4);
D5 = wrcoef('d',C,L,'coif5',5);
%Displaying the Results of a Multilevel Decomposition.
subplot(3,2,1); plot(A5);
title('Approximation A5')

subplot(3,2,2); plot(D1);
title('Detail D1')
subplot(3,2,3); plot(D2);
title('Detail D2')
subplot(3,2,4); plot(D3);
title('Detail D3')
subplot(3,2,5); plot(D4);
title('Detail D4')
subplot(3,2,6); plot(D5);
title('Detail D5')
l=2%input('what level is the starting level');
m=5%input('what level is the finishing level');
n=5%input('no. of coefficients per level');
nu=m-l+1;
```



```

absd=abs(D);
for r=1:l-1
absd(1,:)=[];
end
absa=abs(A5);
num=zeros(1,nu);
for fg=1:nu

    ask=1%input('window starts from which element nu');
    num(1,fg)=num(1,fg)+ask;
    for vv=1:ask-1
        absd(fg,vv)=0;
    end
end
row=zeros(nu,512);
for k=1:nu
    row(k,:)= row(k,:)+sort(absd(k,:));
end
v=zeros(nu,n);
for h=1:nu
    for g=1:n
        v(h,g)=v(h,g)+row(h,513-g);
    end
end
sumv=sum(v');
mm=zeros(1,nu);
for ee=1:nu
    pow=l+ee-1
    mm(1,ee)=mm(1,ee)+(1/(512/2^pow-num(1,ee)+1));
end
final=1/(sum(sumv.*mm))

```

107.002



4137808